AD-A079 037 MASSACHUSETTS INST OF TECH LEXINGTON LINCOLN LAB F/G 17/9
MILLSTONE HILL RADIO STAR CALIBRATION OBSERVATIONS.(U)
AUG 79 W L OLIVER F19628-78-C-0002
UNCLASSIFIED STK-103 ESD-TR-79-217 NL

1 OF 1
AD A079037

END
DATE FILMED
2-80
DDC

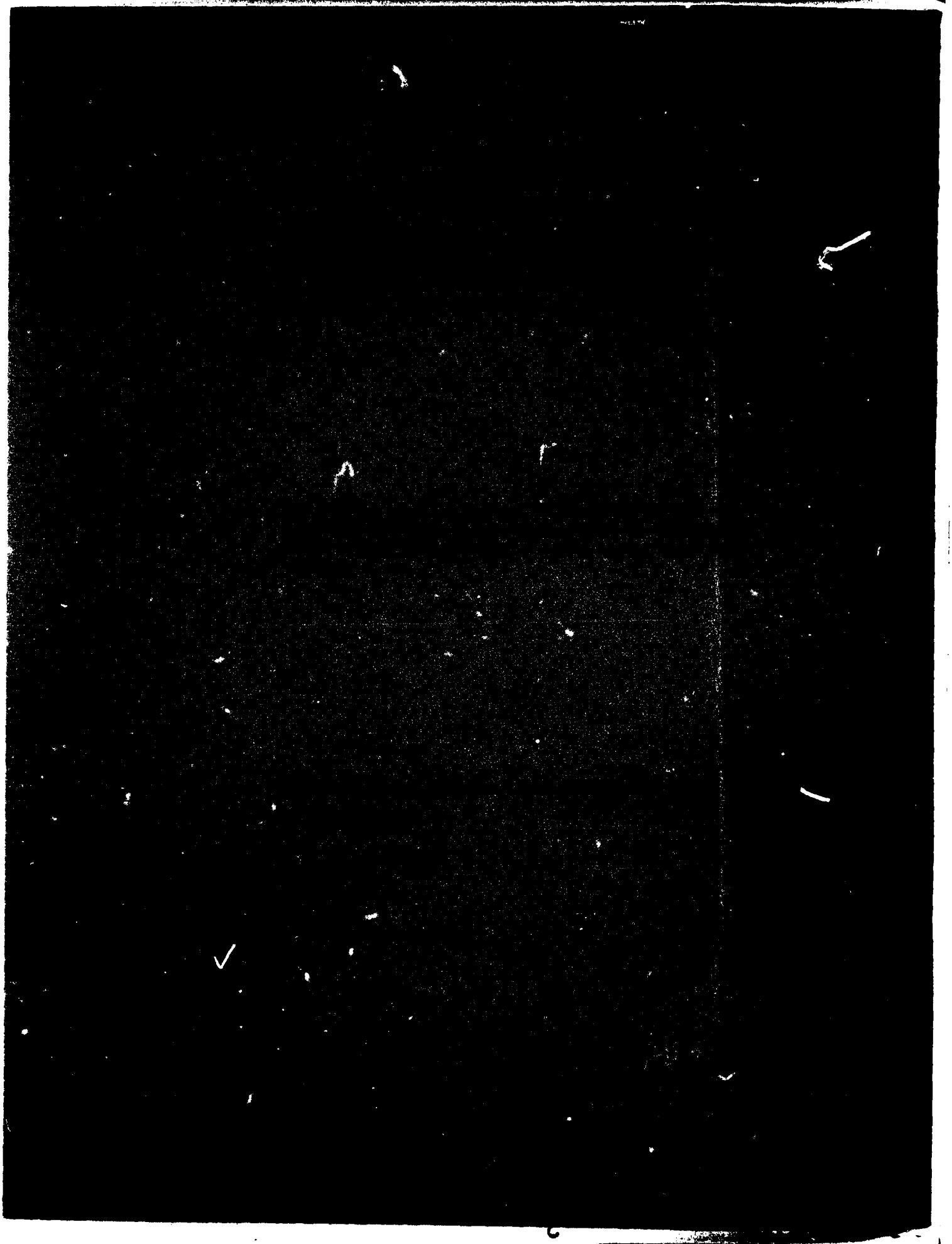

MASSACHUSETTS INSTITUTE OF TECHNOLOGY

LINCOLN LABORATORY

MILLSTONE HILL RADIO STAR CALIBRATION OBSERVATIONS

W. L. OLIVER

Group 91

PROJECT REPORT STK-103

9 AUGUST 1979

LEXINGTON MASSACHUSETTS

ABSTRACT

A comprehensive analyses of all radio-star calibration measurements made since May 1975 with the Millstone Hill Tracking Antenna is described. No evidence is found to indicate that mechanical offsets in the antenna structure have changed during this period. Previous suspicions that such changes might be continually occurring are shown to have arisen from acute mathematical correlation ambiguities encountered in fitting models to the monthly results. In addition, it is found that the high stability of the LED-type encoders installed in November 1977 has virtually eliminated this last source long-term variation in pointing offset. Only known mechanical modifications, causing discrete changes in pointing error model, have caused the pointing-error model to change since this date.

Calibration of the octagonal rail/cam-follower system used by the Tracking Antenna as an off-axis azimuth encoder system is also investigated. Evidence is presented that the primary pointing errors that arise from inaccuracies in this system are due to an offset between the azimuth axis and the geometric center of the rail octagon, an ellipticity of the tower perimeter upon which the rails are mounted, and a slight bowing of the rails, the center offset being an estimated 0.3 mm, the rail geometry being 0.05 mm out of round, and the rails being bowed a maximum of 0.02 mm from straightness. These deficiencies cause pointing errors on the order of 10 mdeg.

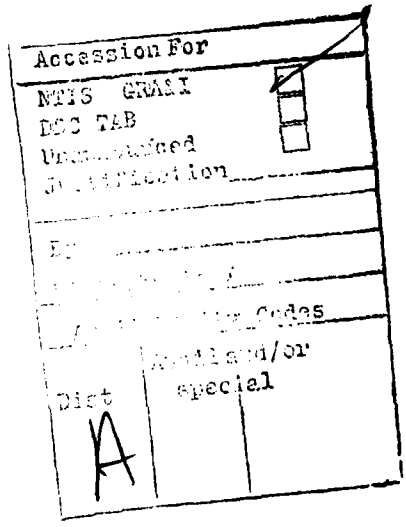

FOREWORD

This report is one of a series prepared under the Satellite Tracking Program. The series reports on a variety of subjects, including: deep space satellite tracking operations and system improvement at the Millstone Hill Radar; results of satellite data analysis; theoretical analyses of radar signal and signature processing; and system planning and concept studies.

The effort covered in this report was sponsored by the Aerospace Defense Command (ADCOM) of the United States Air Force.

CONTENTS

1. INTRODUCTION

The Millstone Hill Tracking Radar was constructed in 1956-1957 initially as a UHF conical scanning test-bed for the Ballistic Missile Early Warning System (BMEWS).[1] The advent of the space age with the launching of Sputnik in 1957 ushered in a period of redirected priorities and rapid advances in radar technology, and as a part of this increased emphasis the Millstone facility has undergone several major and minor modifications to upgrade its capabilities and accuracy. In 1962 the system was converted to monopulse operation at L-band with a Cassegrain optical arrangement and a more accurate surface.[2] From 1969 to 1973, Millstone was engaged in a study of the limitations imposed upon radar systems by naturally occurring propogation effects (e.g., ionospheric and tropospheric refraction, auroral perturbations, ground reflections).[3] The accuracy required for this study necessitated a wide scope of system improvements never envisaged at the start of this study. These included rebuilding the antenna servo control system, installing optical encoders for antenna position readout, stiffening the antenna feed tripod support structure, balancing the antenna, installing antenna tower tilt meters, reducing digital quantization error, installing a new solid-state L-band exciter, using cryogenically-cooled receivers, and providing smooth steering via computer. The product of this overhaul was a system with a 2.75-mdeg digital pointing precision (17-bit encoder) and an optimum attainable repeatability of about 1 mdeg as evidenced by tracks on celestial radio sources.[3] The attainment of such a relative pointing accuracy and repeatability for the Millstone radar has made this instrument a powerful tool for many exercises such as the acquisition and tracking of space objects. There remain some applications, however, for which the additional requirement of <u>absolute</u> accuracy is paramount. The prediction of satellite positions, i.e., orbit-fitting, is a primary example of this need. An attempt to deduce a satellite orbit from observation of only a fragment of its path may produce grossly erroneous orbit predictions if pointing position biases are present.[3] Even for multi-pass solutions, instrumental offsets may cause an incorrect

solution. For such exercises it is necessary to have a measure of the systematic pointing biases in the system and to correct for these biases in processing the observations. Accordingly, several programs have been instituted for absolute calibration of the Millstone system.

Two main types of procedures are used for Millstone antenna calibration. Direct-reading instruments are used where possible to measure time-varying offsets. These include tower tilt, which has been shown to vary significantly in the course of a day, and tropospheric refraction, which varies with atmospheric conditions.[3] Monthly radio star observations are used to determine fixed biases, such as those due to mechanical offsets. This report is concerned with these latter, fixed biases, and it is assumed hereafter that those offsets which are compensated for in real time (tower tilt and refraction) are accurately eliminated in the radio star observations. This report thus considers the radio-star calibration program, concentrating primarily on the information that may be deduced concerning mechanical offsets of the antenna's pointing system.

Section 2 of this report concerns the nature of these fixed antenna pointing biases with an eye toward deriving simple, physically-meaningful, usable pointing error equations which may be easily incorporated for other exercises with the Millstone antenna. Section 3 briefly describes the development of the current radio-star observation program, its capabilities and the data obtainable. Section 4 presents a comprehensive analysis of several thousand radio-star measurements over the last few years and determines the numerical values of the mechanical offsets of the system. Section 5 is a summary.

2. THE NATURE OF ANTENNA POINTING OFFSETS

This section considers the systematic pointing errors to which the Millstone Tracking Antenna is subject. It will be assumed that these are due solely to mechanical offsets in the antenna structure. These offsets are divided here into two categories. First, there is a general class of pointing errors due to axis-misalignments, gravitational deflection,

and encoder biases, to which any antenna mounted in an elevation-aximuth coordinate frame is subject. Second, there is a special type of error peculiarly applicable to the Millstone antenna due to the unique manner in which the azimuth encoding system is mounted off the azimuth axis. These categories are discussed separately below.

2.1 General Class of Pointing Offsets

2.1.1 Axis Misalignments

Any antenna mounted in an elevation-azimuth coordinate frame is subject to pointing errors due to the following axis misalignments[4]

i. Aximuth-axis tilt (failure of the azimuth plane to be horozontal)

ii. Elevation-axis skew (failure of the elevation axis to lie in the azimuth plane)

iii. Collimation error (failure of antenna beam to be perpendicular to elevation axis)

These are illustrated in Figure 1. Azimuth-axis tilt is measured and corrected for in real-time at Millstone and is not discussed further. Elevation-axis skew causes a traverse error

$$\Delta T_1 = \varepsilon \sin E \tag{1}$$

where E denotes elevation angle, while the collimation error is itself a constant traverse error

$$\Delta T_2 = -\delta \tag{2}$$

Projected onto the azimuth plane, these traverse errors become azimuth errors

$$\Delta A_1 = \varepsilon \tan E \tag{3}$$

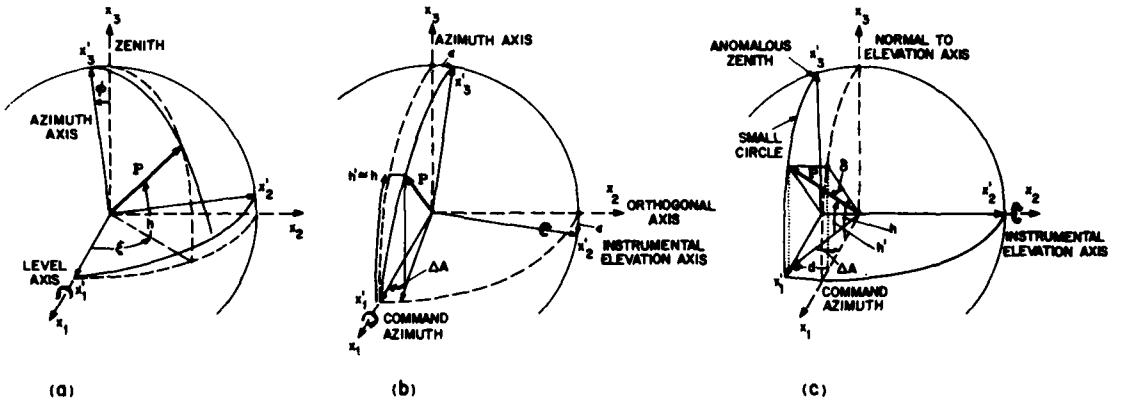

Fig. 1. Illustrations of the pointing offsets due to (a) azimuth axis tilt (ϕ), (b) elevation axis skew (ε), and (c) collimation error (δ).

$$\Delta A_2 = - \delta \sec E \tag{4}$$

These two axis misalignments produce only negligible, second-order elevation errors.

2.1.2 Gravitational Deflection

Massive antennas are subject to significant gravitational deflections of their structures.[4] The symmetry of the Millstone antenna implies that only elevation errors should be produced by this deflection. By resolving the vertical antenna weight vector into components parallel and perpendicular to boresight, one finds a boresight deflection force proportional to the cosine of the elevation angle. Measurements with the Haystack Antenna,[4] however, indicated that the actual deflection angle was linearly related to elevation angle

$$\Delta E = K_E + \beta E \tag{5}$$

Gravitational deflection is expected to constitute the largest source of elevation errors in antennas of this size.

2.1.3 Encoder Offsets

Antenna position readout must be accomplished by some form of encoder measurement of antenna position. There is necessarily some unwanted offset in the positioning or sensor readout of these instruments. This leads to a constant aximuth offset error

$$\Delta A_3 = K_A \tag{6}$$

and a traverse offset of

$$\Delta T_3 = K_A \cos E \tag{7}$$

A similar offset applies in elevation, but such a term would be indistinquishable from the constant term already incorporated in the gravitational deflection error (Equation 5).

2.2 The Millstone Off-Axis Azimuth Encoder System

The original Millstone encoder system consisted of a synchro transmitter/receiver system and a train of gear boxes to transfer the antenna drive-gear position information to a shaft encoder.[2] Gear play and the inability of the repeater to follow the transmitter with sufficient accuracy for purposes of the "propagation experiments" (see Section 1) led to replacement of this system by a new 17-bit digital system connected directly to measure antenna shaft position. For the elevation axis this was accomplished by connecting a "spider" inside the elevation axis torque-tube which drives a shaft coupled to the encoder. The determination of the azimuth position presented considerably more difficulty owing to the fact that the region along the aximuth axis in the vicinity of the bearing is occupied by the waveguide rotary joint, slip rings and R.F. "choke" joints. Thus to place the encoder on the azimuth axis would have required major mechanical changes and much reengineering of the rotary joint structure. To overcome these difficulties, Lincoln Laboratory engineers proposed a novel cam-follower arrangement that allowed the encoder to be mounted off axis.

A plan view of the cam-follower system is shown in Figure 2. The outer cam is an octagon, consisting of eight precisely machined metal bars, or "rails," attached to the rotating structure at the level of the main bearing. Successive rails are mounted alternately above and below one another, so that no true corners are produced where they meet. The angle included by any adjacent pair of rails is adjusted by micrometer to be exactly 135°. The follower unit, shown in Figure 3, is attached to the sidewall of the antenna tower and consists of a small rotating octagon which is held against the inner surface of the larger octagon. In this configuration one rotation of the small octagon is produced for each complete revolution of the antenna/large-cam assembly. Accordingly, the digital encoder can be directly coupled to

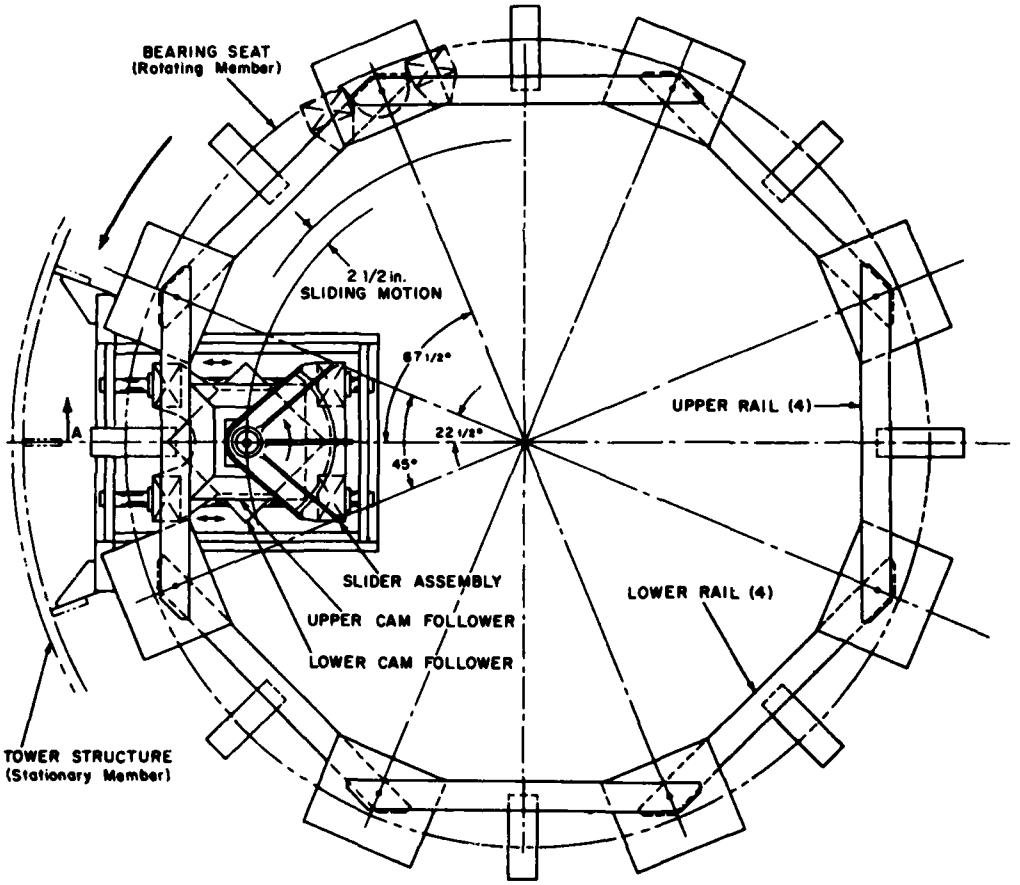

Fig. 2. Plan view of octagonal rail and cam-follower structure.

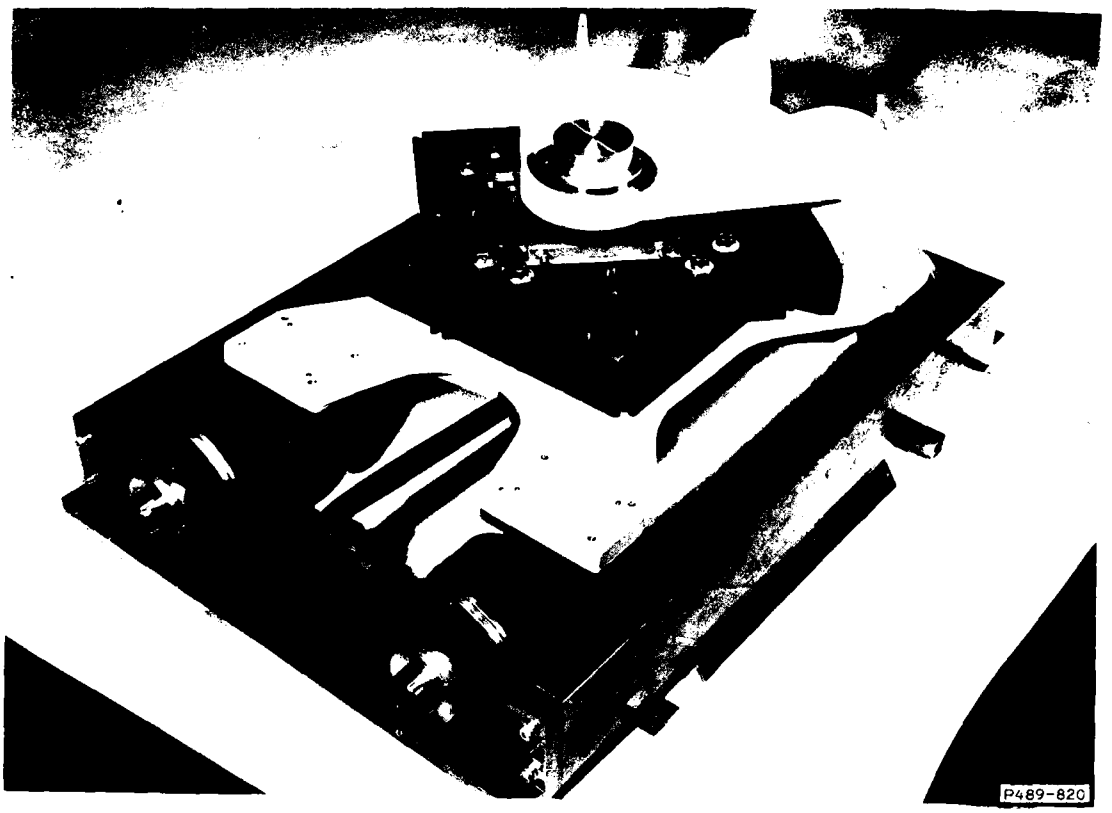

Fig. 3. Photograph of cam-follower.

the shaft of the follower cam and will be turned one revolution for each revolution of the antenna. In order to allow the follower to move back and forth as the large octagon moves by, the follower assembly slides on ball bushings along a pair of cylindrical shafts. A metal tensioning spring was originally used to hold the two surfaces in intimate contact, but was later replaced with a more reliable pulley and gravity shot-bucket combination.

An error will be present in the encoder output whenever there is an unwanted rotation between the encoder shaft and the body being measured. Angle-encoding errors, then, are of two general types: inaccuracies in the mechanical construction of the system, and deformation occurring during normal operation. Preliminary mathematical analysis sets the cam system's allowable structural error to 0.0005°. In that way, the accuracy of the encoders ($\pm 0.00275^{\circ}$) would be the dominant factor in any assessment of azimuth angle-encoding accuracy.

To evaluate the accuracy of the prototype cam arrangement, laboratory bench tests were carried out in which the system was supported on a rotating, air-bearing table with a second 17-bit angle encoder connected directly to the table axis. A digital comparison of the two encoder outputs, one driven directly and the other via the cam system, provided a measure of the accuracy of the cam system, along with information about backlash and other effects. The tests quickly disclosed that several of the rails were distorted and required regrinding. After the regrinding process, the encoders agreed to within 2 encoder bits. This is the maximum resolution of the measurement technique, and indicates that the coupling properly reproduces the angular position of the bearing. These measurements were made with both forward and reverse motion of the bearing in order to detect any backlash effects; other than a one count shift introduced by the measurement system none could be detected. In summary, the laboratory bench tests demonstrated that the system was capable of achieving an rms angle error of about 0.003° (see Ref. 3).

Additional tests were conducted to assess performance as the cam-follower transferred from one rail to the next. At normal tracking rates (~1°/sec) no irregularities were encountered. However, when the rotation rate was increased to 3°/sec, a 2- to 4-LSB error was generated as the corners were traversed.

Upon completion of the air-bearing table tests, the cam-follower system and associated encoders were installed in the Millstone 84-ft tracking antenna. This reconstruction was more difficult, of course, in the cramped confines of the antenna tower. The reconstruction, the uncontrolled temperature environment of the tower, and the greater stresses incurred during antenna operation have the potential of imparting significant rail structure distortions when mounted in the antenna as opposed to laboratory operations.

Two programs were devised to check the accuracy of the installed rail system, one to check the behavior at rail corners and the other to produce a calibration of the rails. A computer program known as RAILROAD was devised to explore the transient behavior of the azimuth encoder as it is rotated through the corners. This program depends on the inertia of the antenna to provide constant angular velocity over short time intervals. If the angular velocity could be held truly constant, then an ideal encoder system would report an antenna position that changed linearly in time, independent of servo sytem action. In a normal sequence, the RAILROAD program fits a single least-mean-squares straight line to all the azimuth values that are collected and produces a plot showing the fitted straight line and deviations of encoded position about the line (see Figure 4). Although some of the deviations shown in Figure 4 may have been caused by actual variations in rotation rate (arising, for example, from wind gusts), the figure nonetheless demonstrates the need for a model of azimuth encoding errors.

Transient steps, caused by the cam's passage from one rail to the next, are clearly visible in Figure 4. These corner-crossing transients may be studied in greater detail employing an expanded version of the RAILROAD plot such as that shown in Figure 5. In this figure the jumps in position at the rail corners are clearly visible. In addition, Figure 5 demonstrates the

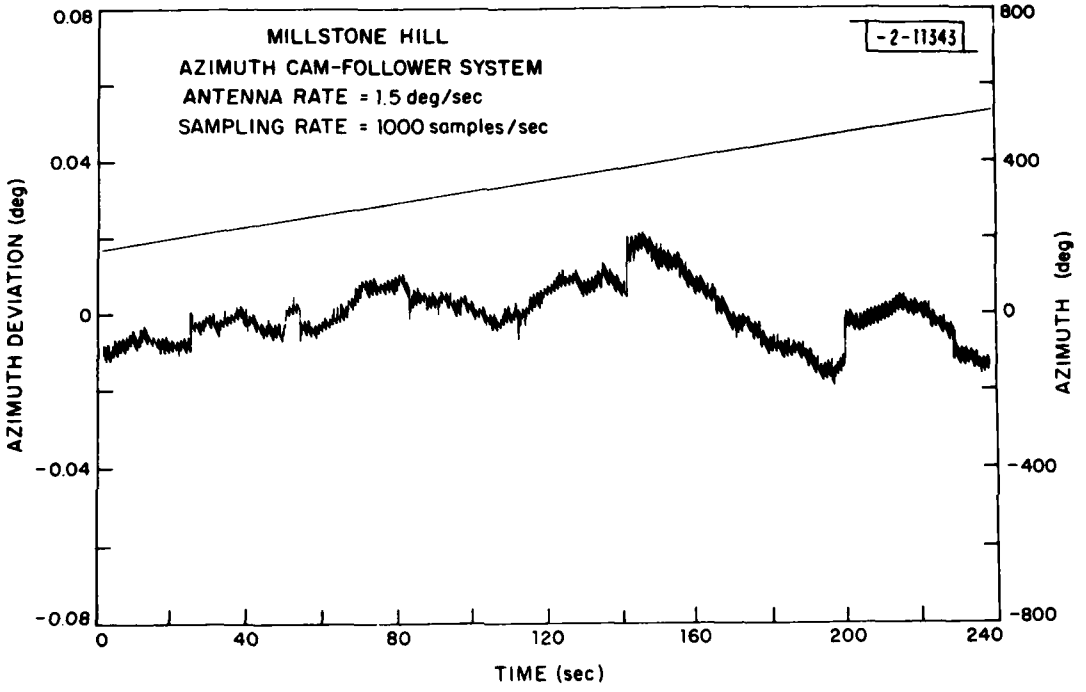

Fig. 4. Sample output from RAILROAD program showing azimuth deviation (raw data, left-hand scale) and azimuth (smooth line, right-hand scale).

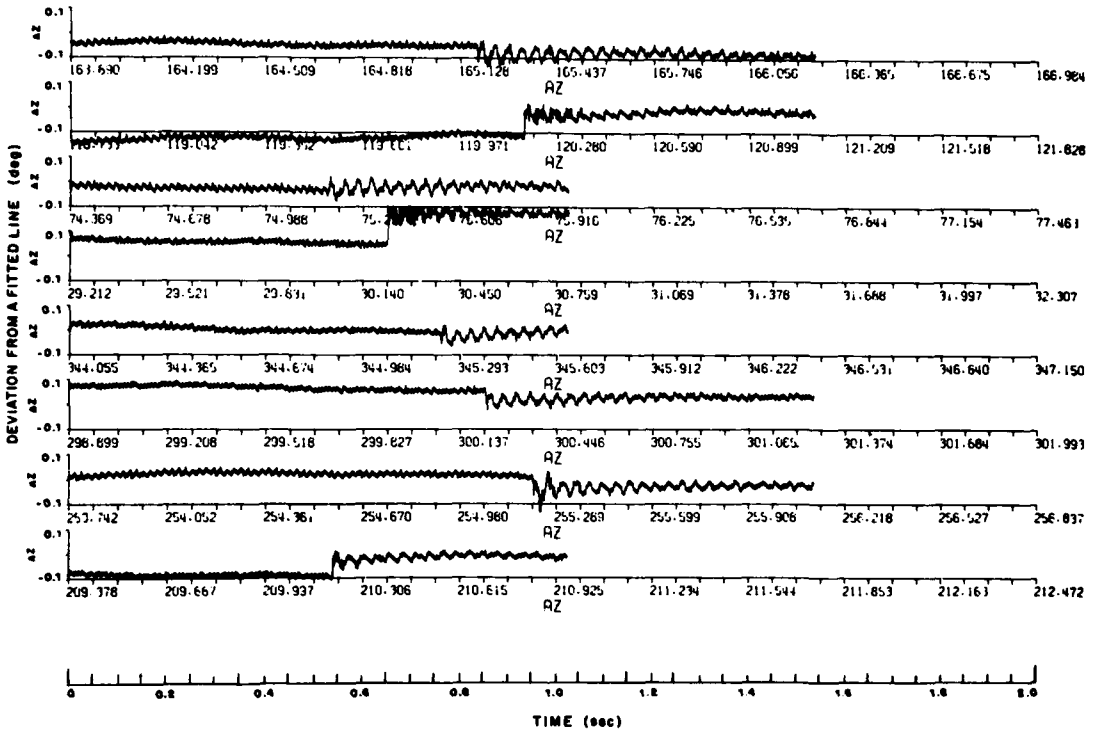

Fig. 5. Expanded RAILROAD plot illustrating performance at rail corners.

presence of oscillations resulting from the cam's contact with a new rail. Repeated measurements have confirmed that these oscillations display a frequency of ~40 Hz and damp out in about 1 second. To date, there has been no effort toward modeling these dynamic errors since they only occur at the relatively infrequent corner crossings.

A second program was devised to determine azimuth errors due to inaccuracies in the overall rail system geometry. This was accomplished with the aid of a precision theodolite to measure true azimuth. First, the theodolite was mounted directly over the azimuth axis and used to measure the positions of 54 selected targets (church steeples, storage tanks, telephone poles, the New England telephone microwave tower in Littleton, etc.) in the vicinity of Millstone. These angles were measured many times, edited, and numerically averaged to obtain a single, best-estimate value for each target. The results of this process may be seen in Figure 6, where we have plotted the deviations of the individual theodolite measurements about the final averages for each of the targets. The combined deviations for all 54 targets have an rms scatter of 3.6 arc-sec (0.001°), which may be taken as an indication of the relative accuracy of the set of final calibration bearings.

To calibrate the rail system employing these known reference targets, provision was then made to view the targets from the azimuth deck through an optical telescope fixed rigidly to the pedestal. On the upper azimuth deck, roughly 4 meters from the azimuth axis, a telescope mounting fixture was permanently attached to the rotating structure, and a telescope was rotating mounted in this fixture and used to make optical sighting on the selected targets. Optical back-sighting checks were also made to insure that the telescope line-of-sight intersected the azimuth axis. The difference between a target azimuth as measured by the theodolite and the azimuth indicated by the azimuth encoder when the telescope was pointing at this target gave an estimate of the azimuth error for that target azimuth. In this manner a complete azimuth error versus azimuth model was formulated.

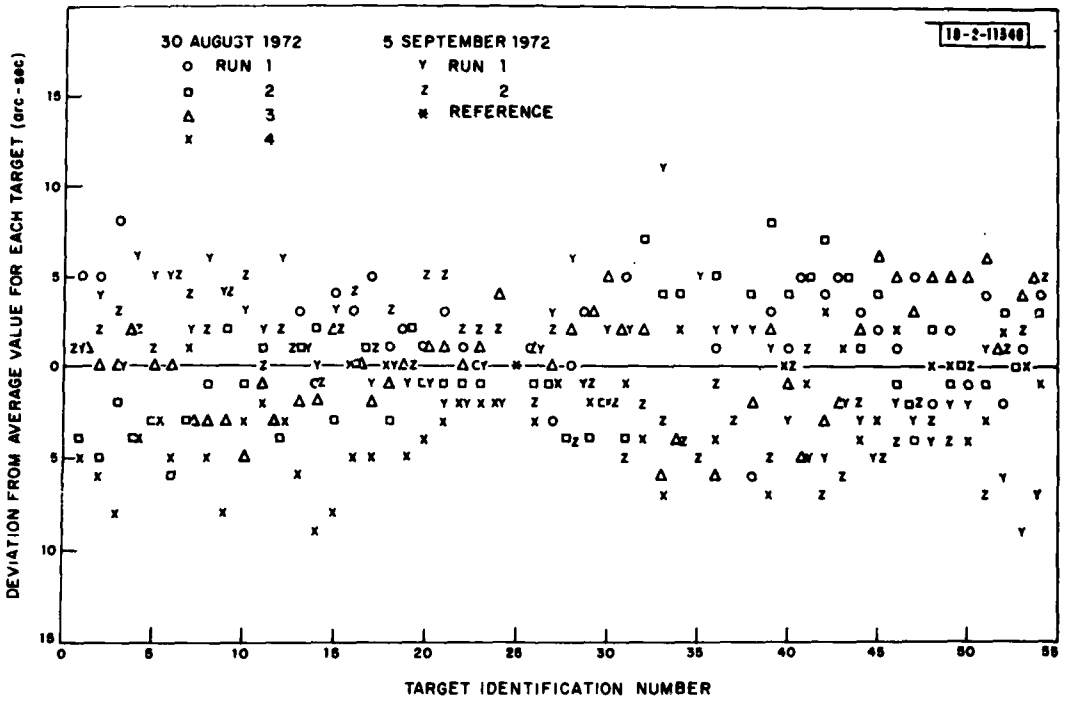

Fig. 6. Deviation of individual theodolite readings from the final average value for each of 54 targets. Overall rms scatter is 0.99 mdeg.

Such telescope measurements were taken on five days in 1972 as listed in Table 1. The September run was the first that was considered sufficiently reliable to be included in the satellite-tracking software. This conclusion was based on the reduced rms scatter of the raw data obtained with these parameters. In contrast to the September observations, the October and November runs were both beset by marginal weather and viewing conditions.

Two interesting points are raised by the 360-degree mean results of Table I, first, that the mean is significantly different from zero, and, second, that this mean may vary by several millidegrees in the course of a month. Several factors may contribute to the mean, such as imprecise absolute azimuth calibration of the theodolite, a slight rotation of the rail network from its intended setting [the rail corners are nominally set at $30^{\circ}11'$ (30.1833°) and every 45° thereafter], imprecise alignment of the telescope, or misalignment of the azimuth encoder shaft or its optical head sensor. As long as all of the potential offsets do not vary during the course of a telescope run, however, the relative azimuth calibration from azimuth to azimuth remains unaffected with only a DC offset preventing absolute calibration. This DC offset is provided by the radio-star observations, discussed in Section 3. The fact that this DC offset drifts from month to month is potentially more troublesome. As the radio star measurements show this same drift, it is surmised that there is some real mechanical or encoder readout variation. It was ascertained that continuous decay caused by darkening of the incandescent lamps used in the optical encoder read-heads was probably the prime contributor to these variations,[3] but it was not possible to rule out the possibility of discrete shifts from time to time in the mechanical structure itself.

The acquisition of the azimuth calibration data from the theodolite and telescope sightings provided the means of formulating an azimuth calibration model. The first model to be devised considered an independent, constant offset for each rail. This amounted to assuming that the rails were each straight but not exactly at angles of 135° apart. Further scrutiny,

TABLE 1

PRELIMINARY LEAST-SQUARES ANALYSIS OF RAW CAM-FOLLOWER ENCODING ERRORS

Date	360-Degree Mean (mdeg)	rms About the 360-Degree Mean (mdeg)	Largest Individual Rail rms (mdeg)
8 June	7.26	6.58	10.08 (Only 28 targets)
12 June	7.60	6.58	10.85 (Only 28 targets)
11 Sept.	10.44	4.86	6.14
20 Oct.	3.75	5.87	5.33 (Hazy)
21 Nov.	4.14	4.09	5.16 (Windy)

however, revealed that there was significant variation along a rail, and subsequently a linear variation along each rail was adopted. This amounted to assuming that the rails were parabolic.

Three of these straight-line models have been produced from theodolite and telescope sighting data, the 72 (or 72-H) model (11 September 1972), the 75 model (19 June 1975), and the 76 model (15 April 1976). The 75 model was deemed to be superior to the 72 model, but the 76 model was deemed inferior to the 75 model primarily due to the windy and hazy atmospheric conditions existing on the days on which the 76 model data were acquired and the accompanying increased data scatter. The 76 model was never actually instituted into any real-time Millstone operation except FLOPET. These models are tabulated in Table 2 and displayed along with the observations in Figure 7. These biases and slopes are suitable for insertion in the formula

$$A = A_E + (B_i + S_i A_E) \qquad i = 1, \ldots, 8 \tag{8}$$

where A represent true azimuth, A_E encoder azimuth, B_i the rail bias (extrapolated to $A_E = 0$) and S_i the rail slope for rail i (azimuth must run from 30.1833 to 390.1833 in this equation). The negative of the term in parentheses has traditionally been called the "rail model," and this is what is shown in Figure 7.

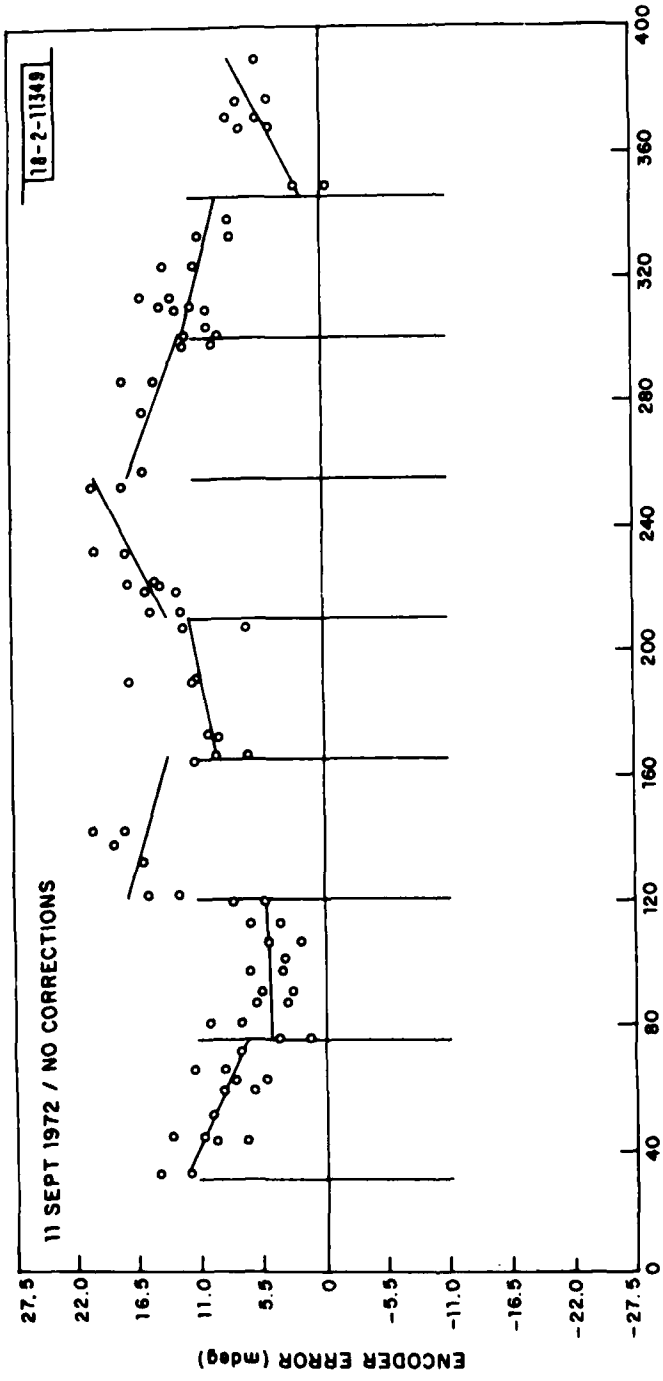

Fig. 7. Rail Models produced by the theodolite-telescope measurements
(a) 1972 model.

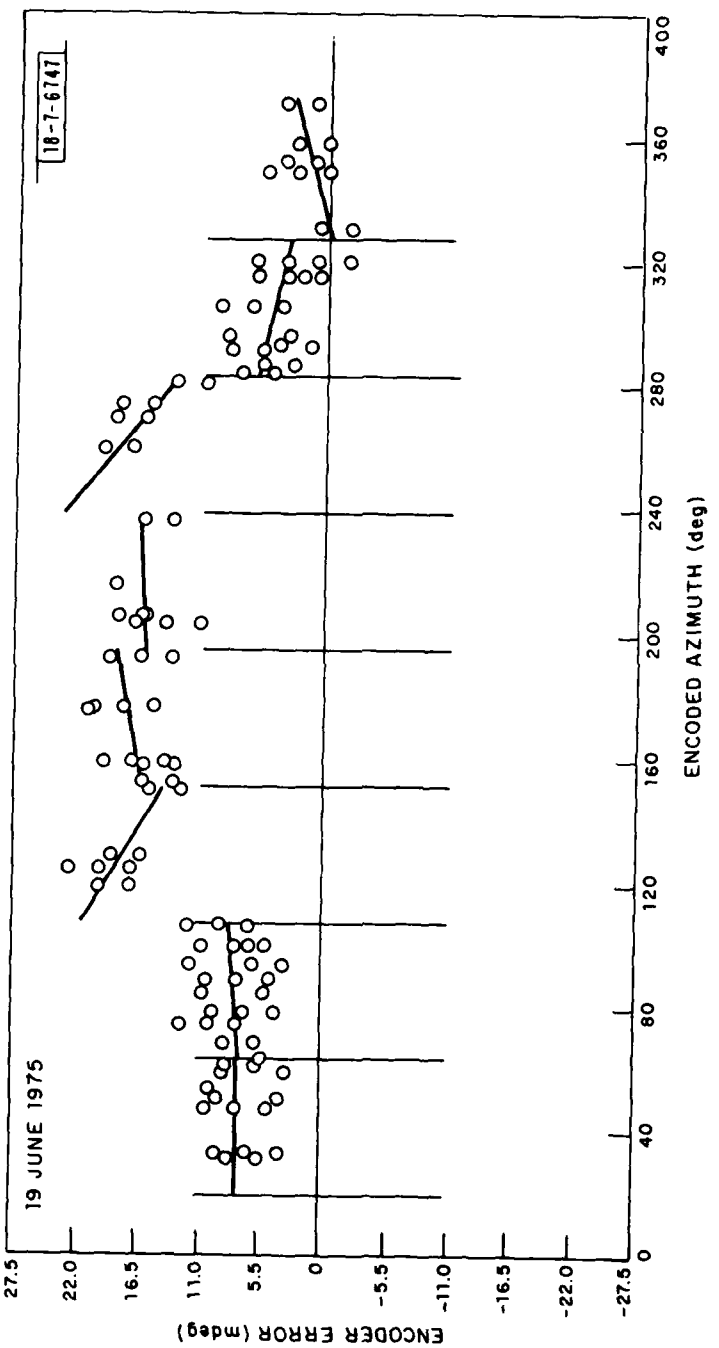

Fig. 7. Rail Models produced by the theodolite-telescope measurements (b) 1975 model.

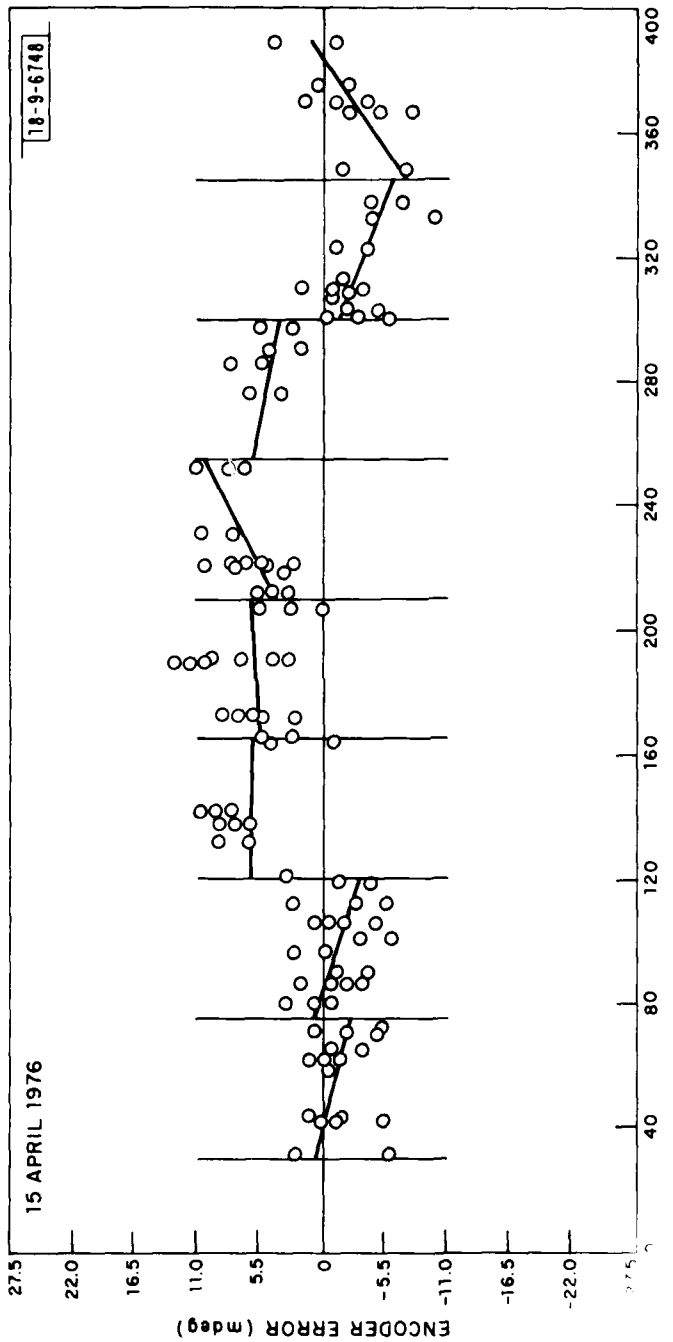

Fig. 7. Rail Models produced by the theodolite-telescope measurements (c) 1976 model.

TABLE 2

THE THREE THEODOLITE-TELESCOPE RAIL MODELS

Rail No.	Azimuth (degrees)	1972 Model Bias	1972 Model Slope	1975 Model Bias	1975 Model Slope	1976 Model Bias	1976 Model Slope
1	30.1833 - 75.1833	-15.75	.1281	-7.41*	-.0007*	-2.51	.0689
2	75.1833 - 120.1833	- 4.40	.0000	-5.67	-.0226	-7.25	.0887
3	120.1833 - 165.1833	-26.37	.0796	-41.20	.1637	-7.61	.0101
4	165.1833 - 210.1833	0.38	-.0556	-7.65	-.0523	-2.65	-.0175
5	210.1833 - 255.1833	17.06	-.1438	-12.46	-.0164	24.41	-.1363
6	255.1833 - 300.1833	-43.09	.1016	-81.69	.2282	-19.26	.0523
7	300.1833 - 345.1833	-32.28	.0684	-25.41	.0636	-30.13	.1056
8	345.1833 - 390.1833	47.86	-.1419	23.43	-.0680	69.92	-.1817

Bias in mdeg

Slope in mdeg/degree

1972 Model used for May - June 1975 FLOPET runs

1975 Model used for July 1975 - July 1976 FLOPET runs

1976 Model used for August 1976 - to date FLOPET runs

*Preliminary bias of 3.81 and slope of -.1786 used for July 1975 FLOPET run

3. RADIO STAR CALIBRATION

3.1 General

Star positions are known through many observations, including interferometer techniques, to perhaps 5 arc-sec accuracy.[5] These absolute reference points provide a very convenient and useful method for calibration large antennas. The difference between the known ephemeris position of a star and the encoder reading of an antenna pointing at that star is a measure of antenna pointing error for that sky (elevation-azimuth) position. By following a number of stars as they move through the sky, one may obtain a complete azimuth-elevation pointing error map. At L-band the number of useful stars is very limited, however, only three major sources being very useful for the Millstone location. Listed below are the five brightest sources, their temperatures and diameters.[6]

Source	Temperature (K)	Diameter Arc Min
Cassiopeia A	205	4
Cygnus A	135	2
Taurus A	84	4
Orion	38	6
Virgo	15	5

Virgo has been tracked in the past, but the results were deemed useless for calibration purposes. To the author's knowledge Orion, has never been tracked for this purpose. The star calibration program at Millstone is programmed to locate and track any of these five stars, plus the star with catalog number 3C273B, upon request. Figure 8 shows the sky coverage afforded by the motions of Cassiopeia A, Cygnus A, and Taurus A.

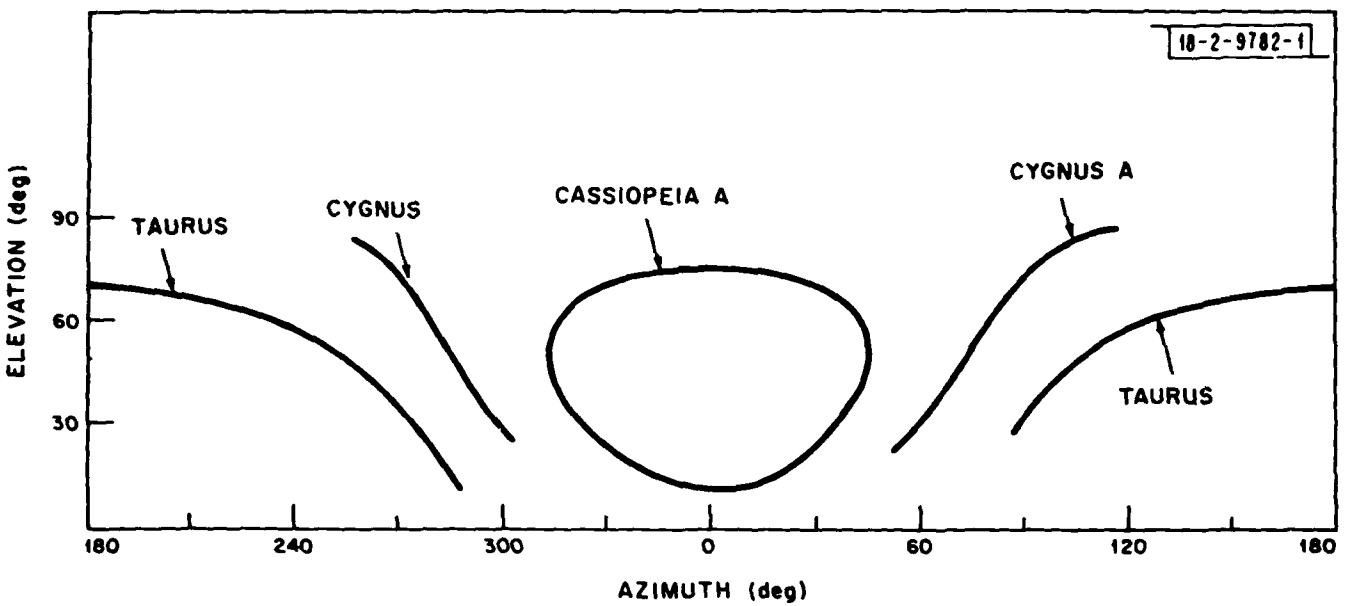

Fig. 8. Sky coverage afforded by tracking the three brightest radio stars from Millstone.

3.2 MOPET Program[3]

The standard L-band monopulse tracking receivers at Millstone will autotrack strong radio sources. However, useful angle data cannot be collected while simply autotracking for two reasons: the receivers are narrowband and the star noise is weak (often less than the receiver system noise). Thus the tracking is noisy ($\sim 0.01^{\circ}$ rms) unless the tracking-loop time-constants are increased to tens of minutes in some cases. This would give few independent measurements during any period set aside as calibration time. Measurements may be made in less time, however, by using wider predetector bandwidths. Accordingly, a modified system, having a wider sum channel and auxiliary angle detectors at the 30-MHz intermediate frequency point where the bandwidths are approximately 1 MHz (2000 times wider than the normal L-band tracker), is used for star tracking. Tests show that $\sim 0.002^{\circ}$ changes can be observed in a few seconds with the modified system.

The original star calibration program at Millstone incorporating these modifications was known as MOno Pulse Error Tracking (MOPET). For MOPET operations the antenna was placed under the control of the XDS computer, which commanded it to follow the known position of one of a number of bright celestial radio sources having small angular diameter (usually Cassiopeia A or Cygnus A). The computer then superimposed on this sidereal motion a scan in either azimuth or elevation.

For a monopulse receiver the error voltage during a scan across a source changes from positive to negative (or vice versa) as the source is traversed, being ideally zero when the source is in the middle of the antenna beam and falling to zero as the source moves out of the beam (Figure 9). Because of a possible DC offset in the error voltage output, however, the source position should be taken to be that position attained when the star is in the beam and the error voltage is equal to the DC offset measured when the source is completely out of the beam. This is achievable by fitting straight lines to the error voltage versus scan position both along the base line and in the transition region as shown in Figure 9. The intersection of these lines is the desired source position estimate.

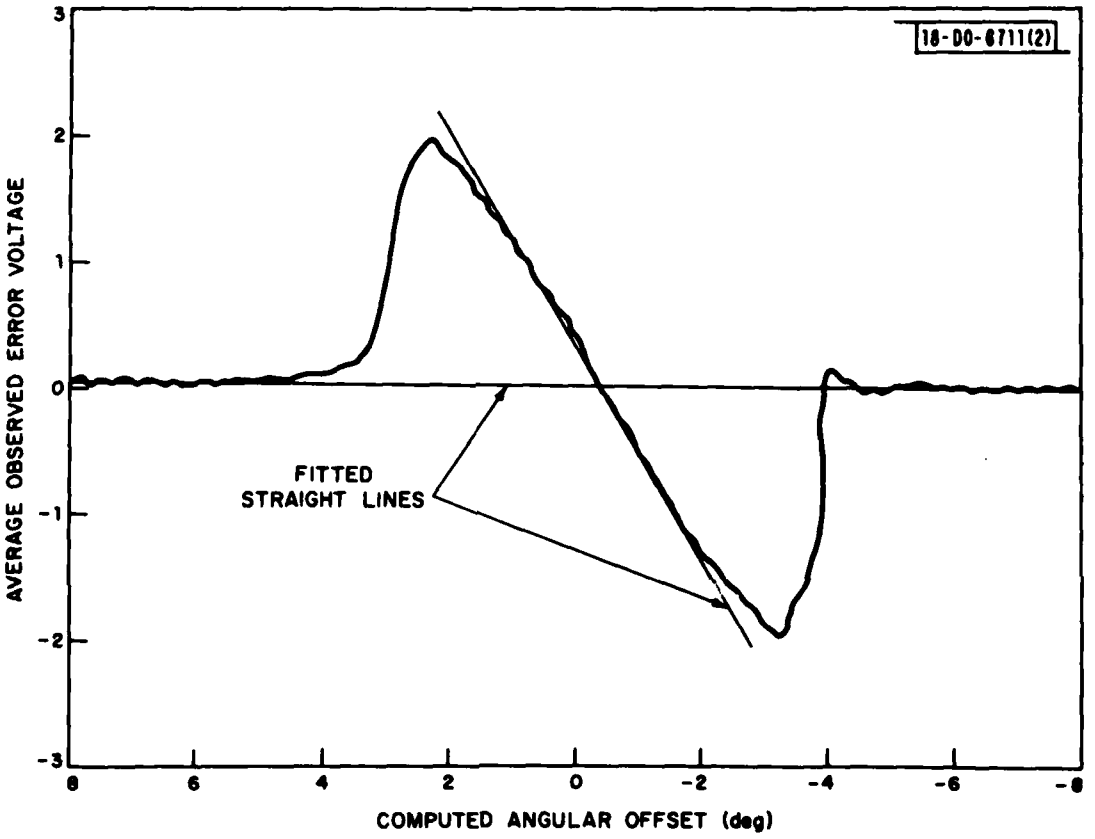

Fig. 9. Illustration of the monopulse error voltage curve as a function of offset from source center (drawing actually corresponds to wide-beam UHF system no longer in use) and the line fitting method employed to determine source position for MOPET.

DC offsets are, in fact, present in the system (contributed to by mixer unbalance, operational amplifiers, pickup, etc.), causing much of the MOPET scan time to be spent off the star to measure them. More detrimental, however, was the discovery that this baseline drifted with gain fluctuations, etc., to an extent that these source position estimates were significantly biased. Overall, these problems caused the theoretical accuracy of the system of 0.25 mdeg for 3 seconds integration time on Cassiopeia A to be degraded to 3 mdeg at best.

3.3 FLOPET Program

As a cure for many of these shortcomings, it was decided to modulate the error signals so that they might be distinguished from unwanted DC offsets. This method was implemented by modulating the phase of one local oscillator in the error channels between 0° and 180°. The component of the error signal at the output of the angle error detectors due to a real error signal then alternates in sign. Any other output voltage component that arises from the sum channel or pickup after the phase "flipping" point will appear as before - a DC voltage. After amplification, filtering, sampling, and analog-to-digital conversion, the modulated component of the sampled voltage is readily extracted by computer processing. This system was termed Flipped Local Oscillator Phase Error Tracking (FLOPET).

With this phase-switched receiver system, DC offset variations introduce only second order effects. Moreover, it is no longer necessary to establish "baselines" by scanning across the source; a small offset is indicated by a small alternating voltage, zero offset ("boresight") by zero alternating voltage. The boresight position may be estimated by error voltage readings and angle encoder readings all taken with the radio star in the beam, permitting more efficient use of available integration time. This also made a reduction in bandwidth possible without sacrificing angle sensitivity.[3]

The improvement due to the flipping process has enabled the L-band system to produce repeatable results exhibiting an uncertainty of $<0.001^{\circ}$ rms in two-minute runs and clearly showing errors other than the thermal noise limitations. For example, the azimuth encoder angle offsets at "rail"

corners are apparent, and the tilting of the antenna tower was evident before the real-time tiltmeter corrections were instituted.

The FLOPET program was developed as part of the Propagation Study (see Section 1) to the point of having the program operate reliably and obtaining a few test measurements, but it was not used in a routine manner until much later, in May 1975, to attempt to monitor system pointing performance on a regular basis. A major diagnostic improvement was implemented at this time in the form of a real-time scope display of the error voltage vectors, pointing positions, refraction and tilt corrections, etc., to monitor the program performance. One result of this feature was the recognition that many stray position estimates were the results of bursts of interference, and an interference filter was subsequently implemented.

Another feature of FLOPET added at this time was the capability of a "tracking" mode in addition to the "scanning" mode. In the scanning mode, FLOPET determines the error voltage at three points along the error voltage curve and fits a straight line to these points to estimate error null position. This is similar to the MOPET type of scan as shown in Figure 9 but with only three points obtained in the transition region (and the DC bias eliminated). If the error voltage curve is not precisely linear in the transition region, however, an error in the null estimate could occur if these three points were not centered closely around the null. Improper initial estimates of the star position before a scan have, in fact, resulted in frequent cases of an error of this nature. Nevertheless, information from these faulty scans has always been adequate for a correction for the second scan such that subsequent scans could produce valid null estimates.

To check the affect of the assumption of transition region linearity, the tracking mode was implemented in which error signals were continually used to keep the beam on the star. This method requires only an approximate knowledge of the transition slope, as obtained from a prior scan, to allow the error voltage information to be interpreted in terms of an angle error.

The linearity restriction is removed in this case. A comparison of scanning and tracking results has not shown any systematic differences, and it has been concluded that except, perhaps, for an occasional bad first scan, FLOPET operates on a linear portion of the error voltage curve. Both scanning and tracking exercises have been retained in routine FLOPET operations.

3.4 FLOPET Observations

Since May 1975, the FLOPET program has been run routinely, nominally monthly, to monitor system pointing performance. Normally, observations on the three strong stars Cassiopeia, Cygnus, and Taurus are sequenced through according to visibility. Sample Virgo observations have not proved useful; Orion and 3C273B, through written into the software, have not been observed. Generally, an azimuth scan followed by an elevation scan will be repeated four times and five tracks will follow, each scan or track being on the order of one minute duration. The operator, however, is free to choose the source, integration times, and number and type of observation as he pleases. Due to the overhead of program setup and checkout, operator intervention, and antenna positioning, a typical FLOPET operation of 16 hours, from 1600 LT to 0800 LT, accumulates on the average of some 300 independent elevation-traverse offset measurements. The main daylight hours are avoided due to possible solar sidelobe contributions.

4. MECHANICAL OFFSETS DETERMINED FROM FLOPET OBSERVATIONS

4.1 Monthly Results, May 1975-May 1978

FLOPET has been run nominally once a month since May 1975. Initial consideration is given here only the period through May 1978 as hardware changes made prior to the June 1978 run caused major departures in the pointing-error models. The post-May 1978 period is considered in Section 4.4. After each FLOPET run the results are edited by hand, referring to a strip chart recording of various system parameters (error voltages, sum channel output, tilt corrections, antenna command, wind speed) and log book notations as suspicious results arise. These results are then plotted and

fitted separately in elevation and traverse according to the error model formulations introduced in Section 2. In elevation the errors are primarily due to gravitational deflection of the antenna structure in a manner difficult to predict theoretically. A linear error versus elevation model has been used for the Haystack antenna,[4] but a parabolic model is necessary to fit the Millstone results

$$\Delta E = K_E + \beta E + \gamma E^2 \tag{9}$$

In traverse the fitted model is

$$\Delta T = \varepsilon \sin E - \delta + K_A \cos E \tag{10}$$

where ε is the elevation-axis skew, δ is the collimation error, and K_A is the azimuth encoder offset. The monthly results for K_E, β, γ, ε, δ, and K_A are shown in Figures 10 and 11. These results merit careful consideration. K_A is an encoder offset and K_E is the sum of an encoder offset and the gravitational deflection error at E = 0. During maintenance checks on these encoders, continual adjustments have been made to compensate for continuous decay caused by darkening of the incandescent lamps (until November 1977, when LED units were installed - see Section 4.4) such that some arbitrary variability in K_E and K_A could be expected. On the other hand, β, γ, ε, and δ should represent fixed mechanical properties and therefore be relatively invariant from month-to-month. In fact, great variability is seen in each of these parameters, and, moreover, these variabilities are highly correlated. These variabilities were recognized early in the program, and suspicion arose that they represented true variations in mechanical offsets. These monthly results were not, however, routinely plotted as shown in Figures 10 and 11 nor were the error statistics examined for each monthly run and the high correlation between parameter variations was not recognized until very recently. Spot checks of these error statistics show that correlation coefficients of 98%

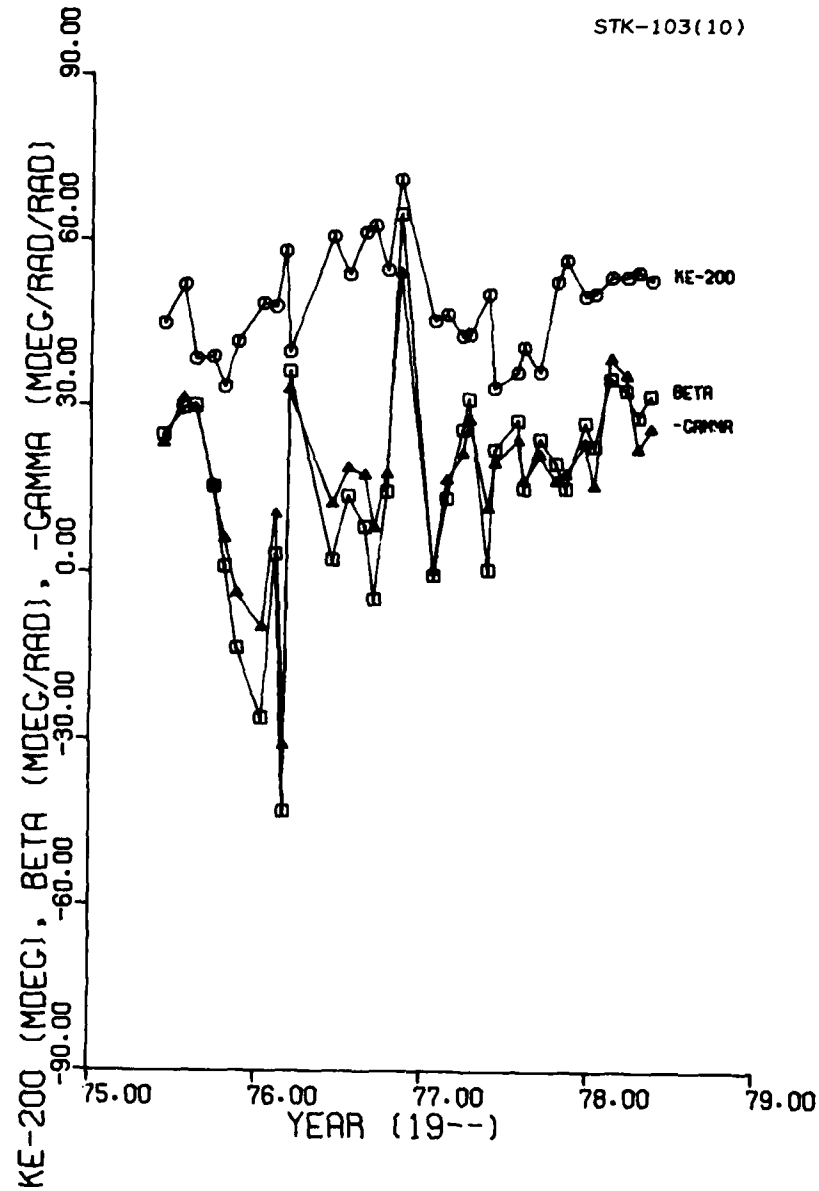

Fig. 10. K_E, β, and γ results determine from the independent monthly analyses of FLOPET data, May 1975 - May 1978.

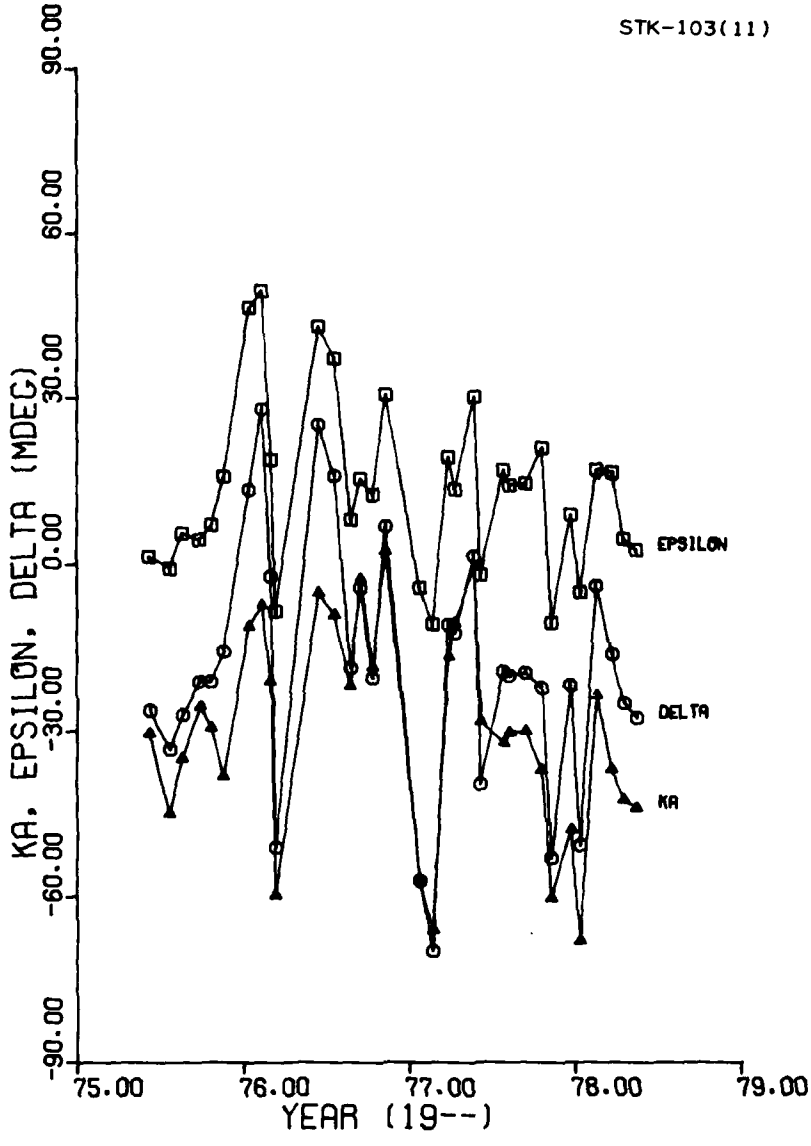

Fig. 11. Same as for Figure 10 for K_A, ε, and δ.

have occurred in these monthly analyses. A 100% correlation coefficient, of course, would mean that any change in one of these parameter may be precisely compensated for by an appropriate change in the other without affecting the total model at all, such that the result for either parameter is totally meaningless by itself. There must be strong suspicion, therefore, that the large monthly variations depicted in Figures 10 and 11 are not real but rather result from mathematical ambiguities. If the month-to-month correlations had been large but the correlation coefficients between parameter had been small for each monthly run, then there would be evidence of true monthly variations in the mechanical offsets.

For completeness, it should be mentioned that a high correlation coefficient between two parameters is not always a sufficient test for mathematical ambiguity. This only detects dependencies between pairs of variables. There may be three variables having near mutual dependence whereas no two of the variables are nearly dependent. Consider, for example, the 3 x 3 matrix with unity diagonal and -.49 off diagonal, which could possibly occur as a correlation coefficient matrix. As no off-diagonal element is near 1 or -1, no two paramters are closely correlated, but the matrix is near singularity. If the values -.49 are changed to -.50, singularity does occur, and perfect mutual dependence of the three components is attained. Thus, in our particular case with the FLOPET results, the mutual dependence of ε, δ, and K_A in Figure 11 may be more detrimental than the seemingly more pronounced mutual dependence between β and $\dot{\gamma}$ in Figure 10.

In addtion to the mathematical arguments against the reality of monthly variations appearing in Figures 10 and 11, physical arguments may be invoked. Is is reasonable that three physically-meaningful and independent parameters (such as ε, δ, and K_A) should vary in well-coordinated unison, especially when one of these parameters (K_A) is no more than a technician's trim adjustment to an external slave mechanism?

4.2 Comprehensive Analysis, May 1975 - May 1978

The present study began as an exercise to determine if the simultaneous consideration of many months of FLOPET results could enable more useful information concerning system pointing offsets to be deduced than the previous method of considering each month's observations independently. To this end all FLOPET measurements have been considered as one large set and a single model fitted to this set. The May 1975 - May 1978 data set consists of 7073 offset measurements in each elevation and traverse.

The comprehensive analysis started with the assumption that the antenna offset parameters were invariant with time with the exceptions of the encoder offsets K_E and K_A, which might vary according to continual trim adjustments. Thus parameters β, γ, ε, and δ of Equations 9 and 10 were assumed to be fixed while K_E and K_A were allowed independent monthly variations. It was also hoped that the accumulated mass of data would be sufficient to allow a rail model determination, though FLOPET was not designed for this purpose. A linear rail model of the form of Equation 8 was also assumed to be fixed. The elevation and traverse errors were then modeled as

$$\Delta E = K_{Ei} + \beta E + \gamma E^2 \tag{11}$$

$$\Delta T = \varepsilon \sin E - \delta + K_{Ai} \cos E + (B_j + S_j A) \cos E \tag{12}$$

for run index i covering the monthly FLOPET runs and rail index j = 1, ..., 8. It should be mentioned that a rail model correction is routinely applied in the FLOPET real-time program and that this correction (which took four separate forms during the period under consideration) had to be undone before Equation 12 could be fitted to the data.

One problem immediately arose with Equation 12. It can be easily seen that if some constant is added to each of the K_{Ai} and subtracted from each of the B_j, the model remains unchanged. That is, it is impossible to distinquish between a rotation of the entire rail structure and a rotation of the encoder connected to this structure. Thus, it was necessary to set some fixed reference for this model, and $K_{A1} = 0$ was arbitrarily chosen. All other K_{Ai} and the rail model are then meaningful only with respect to this reference.

The mechanics of making this fit posed some problems due to the large data set and number of free parameters involved. All available package routines would overrun the XDS 9300 memory capacity. To alleviate this problem, a technique utilizing the Givens transform was adopted. This method allows the data to be fed sequentially to the fitting routine without any need of subsequent storage. Computer core usage may thus be independent of data set size. In addition, any fit may be updated by this method as new data becomes available simply by recalling the previous results and feeding in the new data. Data may also be edited out of a fit simply by refeeding the data to the program with the negative of the weight originally used. Furthermore, this method is as accurate and as fast as any other existing method. This technique has proved so useful that Appendix B has been devoted to a presentation of its use.

The results of the fit of the elevation error equation (11) to the May 1975 - May 1978 data set are the values

$$\beta = 20.17 \text{ mdeg/radian}$$
$$\gamma = -20.78 \text{ mdeg/radian}^2$$
$$\rho_{\beta,\gamma} = -.972$$
$$\text{s.d.} = 4.57 \text{ mdeg}$$

and the K_E values as shown in Figure 12. $\rho_{\beta,\gamma}$ is the correlation coefficient between β and γ, and s.d. is the standard deviation betwen the fitted model

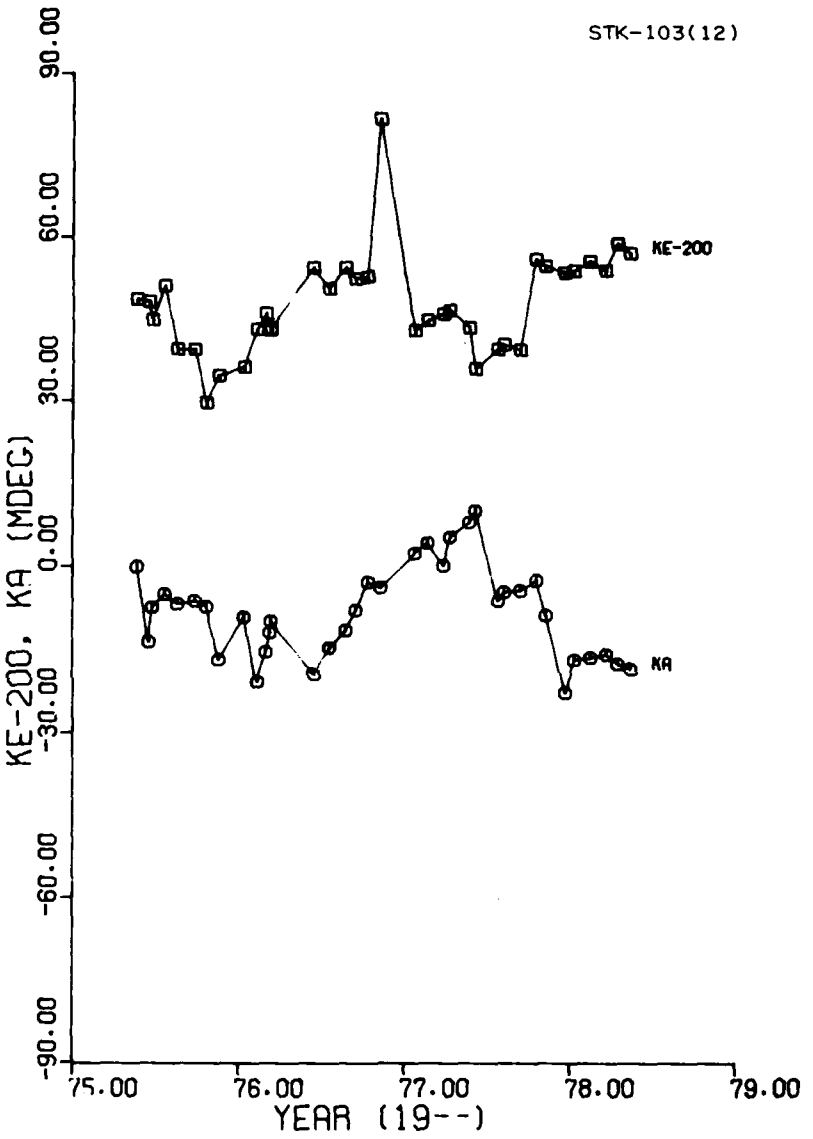

Fig. 12. K_E and K_A deduced by the comprehensive analysis of the May 1975 FLOPET data (Rail Model 1 used in deriving K_A).

and the data. Comparing these results with the monthly results of Figure 10, we see that the K_E variation is somewhat smoother for the comprehensive analysis and the β and γ from the comprehensive analysis could be fairly well represented by averages of the monthly results. The magnitude of $\rho_{\beta,\gamma}$ is so near unity, however, that the β and γ results are not trustworthy as measures of mechanical offsets. There is probably a sizable range of values for either β or γ within which the other parameter can be adjusted to give a good fit to the data also.

Figure 13 shows all of the raw data points for the set after K_E has been subtracted for each run compared with the curve $\beta E + \gamma E^2$. The fit to the data seems fairly uniform except, perhaps, for an inability of the parabola to follow the dip of the data at the lowest elevation angles. Much of the data for low elevations has, in fact, already been edited out due to erratic behavior common for these near-ground observations. Much of this is due to reflections of the source radiations from the ground into the antenna, giving an apparently low position location. An overestimate of tropospheric refraction would produce the same tendency. The pattern at low elevation angles, however, is by no means consistent, and the quality and quantity of these data do not provide hope that any useful conclusion on thus topic may be drawn from the FLOPET program.

Figures 14, 15, and 16 break up Figure 13 star by star with the same model being plotted in each case. The Taurus measurements near 69 degrees are separated from the curve by a significant amount. This anomoly is unexplained (but see Section 4.5 concerning star background noise).

The results of the fit of the traverse error equation (12) to the May 1975 - May 1978 data set are the values

$$\varepsilon = 8.79 \text{ mdeg}$$

$$\delta = -24.00 \text{ mdeg}$$

$$\rho_{\varepsilon,\delta} = 0.978$$

$$\text{s.d.} = 4.24 \text{ mdeg}$$

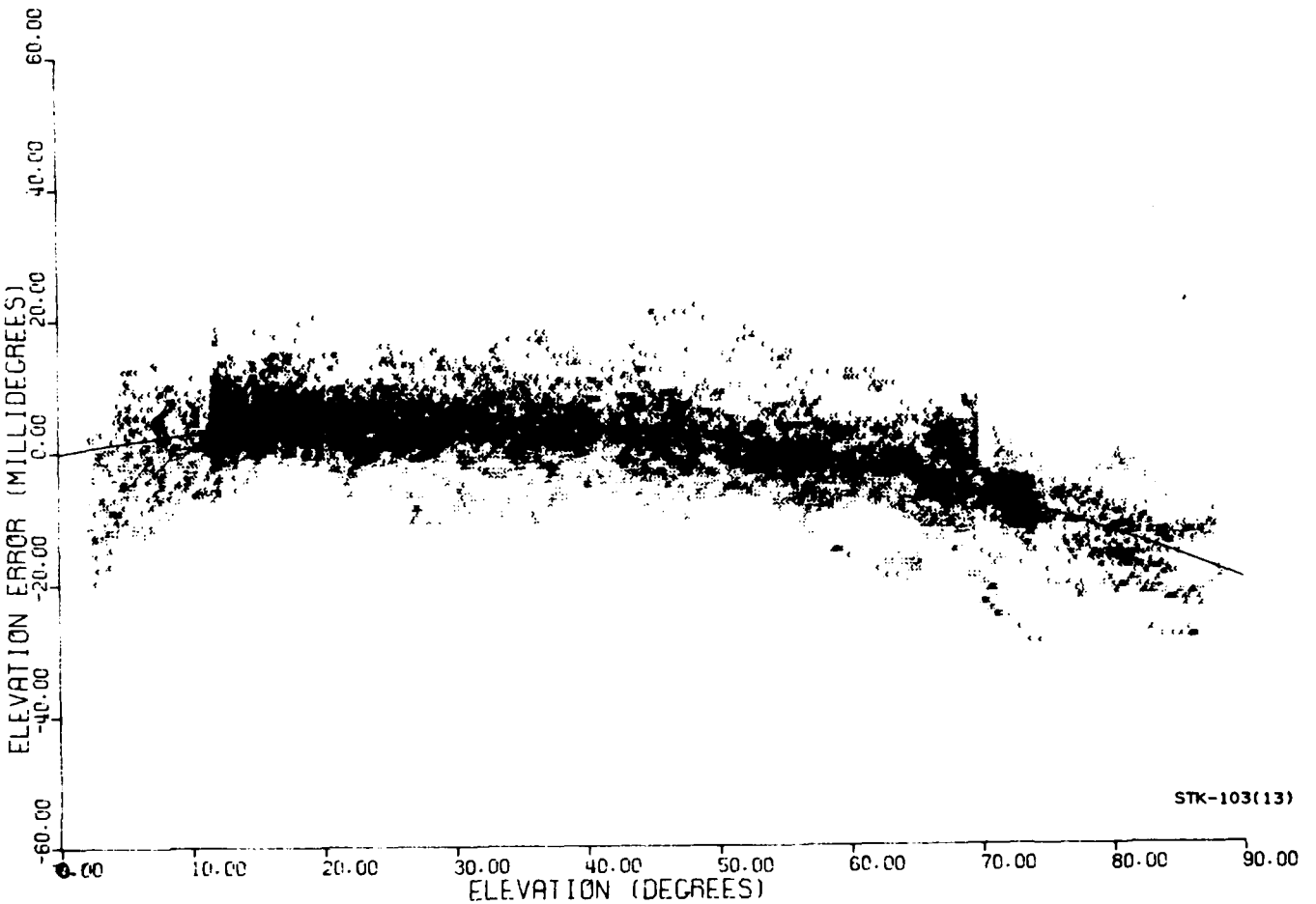

Fig. 13. Comprehensive analysis elevation error model compared with the data after suppression of the monthly offsets K_E.

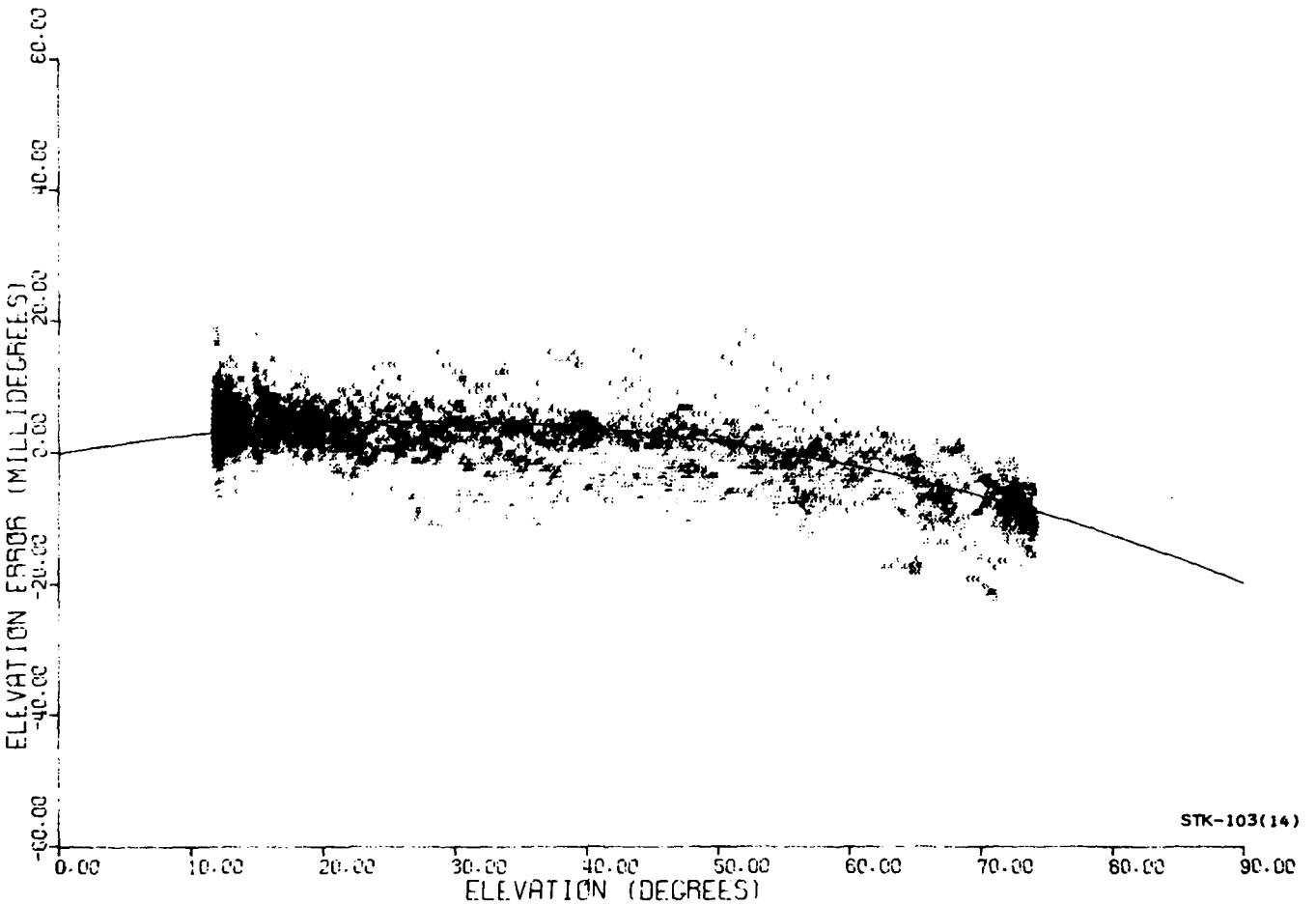

Fig. 14. Same as Figure 13, showing only Cassiopeia data.

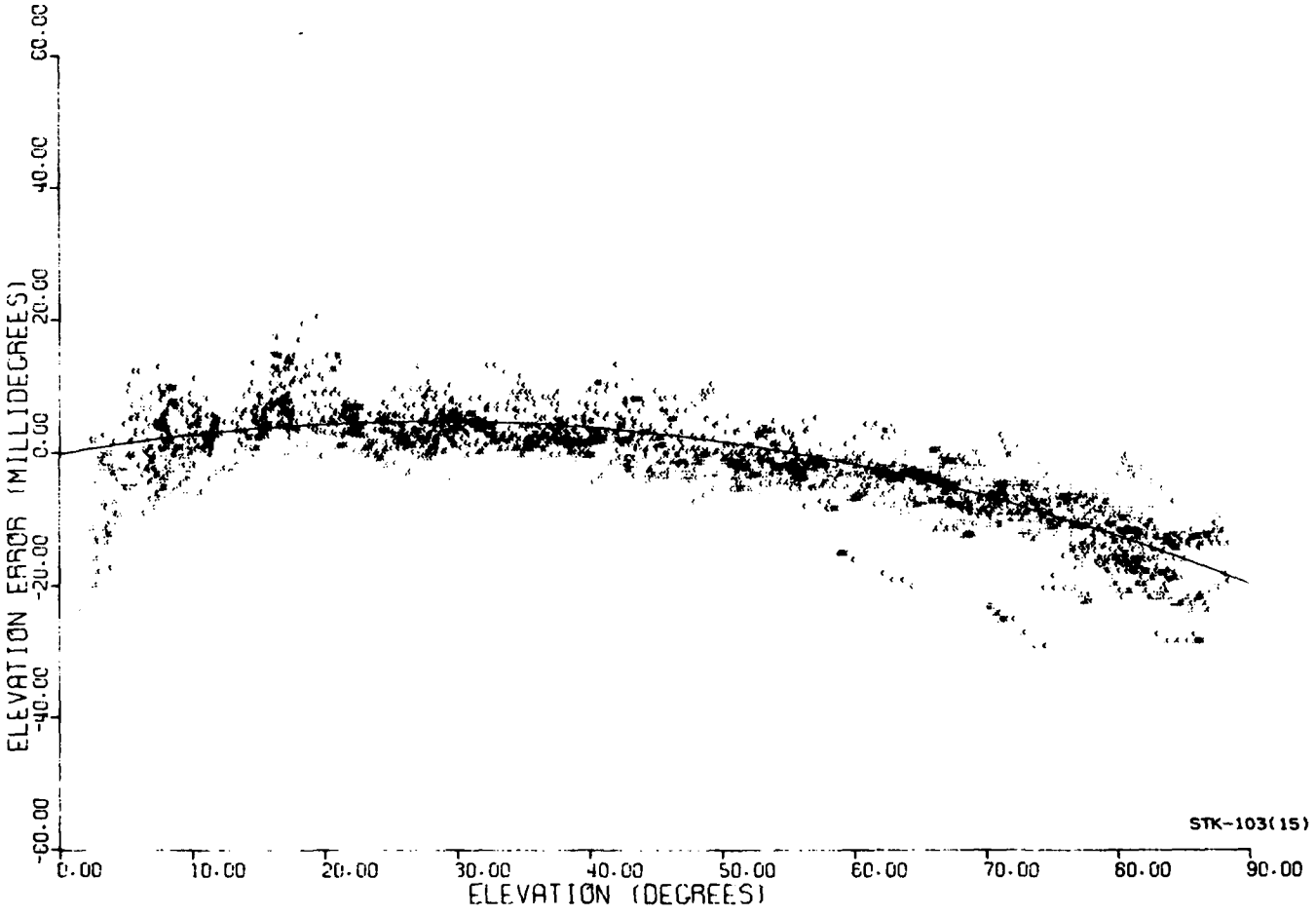

Fig. 15. Same as Figure 13, showing only Cygnus data.

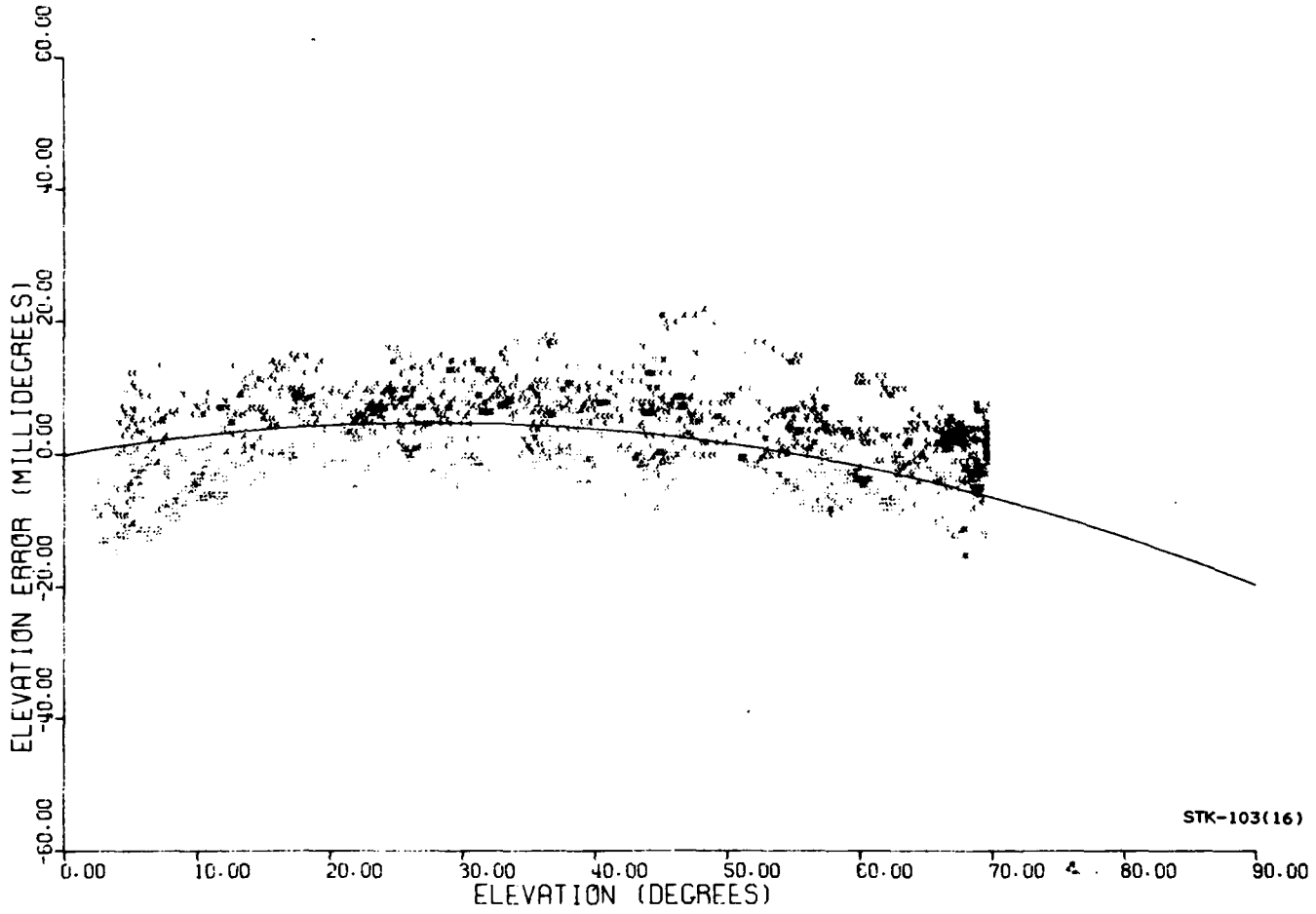

Fig. 16. Same as Figure 13, showing only Taurus data.

and the K_A values as shown in Figure 12 (the rail results are discussed in Section 4.3). Comparing these results with the monthly results of Figure 11, we see that the K_A variation is much smoother for the comprehensive analysis and that ε and δ from the comprehensive analysis could be fairly well represented by averages of the monthly results. $\rho_{\varepsilon,\delta}$ is so near unity that the δ and ε values cannot be taken as good estimates of the actual mechanical offsets. Figure 17 shows all of the raw data points for the set after $K_A \cos E$, the rail model correction, and $-\delta$ have been subtracted, compared with the curve $\varepsilon \sin E$, and Figures 18, 19, and 20 break this display up by star.

An additional exercise was made with these data to investigate further the ambiguity in the $K_A - \varepsilon - \delta$ determination. The model curve 8.79 sin E was evaluated at 5 degree increments from 5 to 85 degrees elevation, and this set of points was then fitted by a curve $a + b \cos E$ with the results being a = 10.92 mdeg and b = -8.16 mdeg as shown in Figure 21. The purpose of this exercise is to show that, at least away from the more sparsely populated elevation limits, completely different values of K_A, ε, and δ are capable of producing a good fit to the data. This particular exercise has, in fact, just dropped ε out of the model and found that over a 90 degree sector a constant may be approximated by a sinusoid within an accuracy comparable with the scatter of the traverse error data. This is a clear demonstration of the severity of the mathematical ambiguity encountered in fitting these data.

4.3 Rail Model Results, May 1975 - May 1978

The original rail model conception in 1970 - 1971 contained only an offset per rail under the assumption that the rails were straight but perhaps not set at precisely at 135° at their corners. The theodolite - telescope measurements (Section 2.2) showed that the offsets were not necessarily constant within a rail sector, and a linear offset model along each rail was then adopted. This latter type of rail model has been used to fit the May 1975 - May 1978 data set with the results as shown in Figure 22.

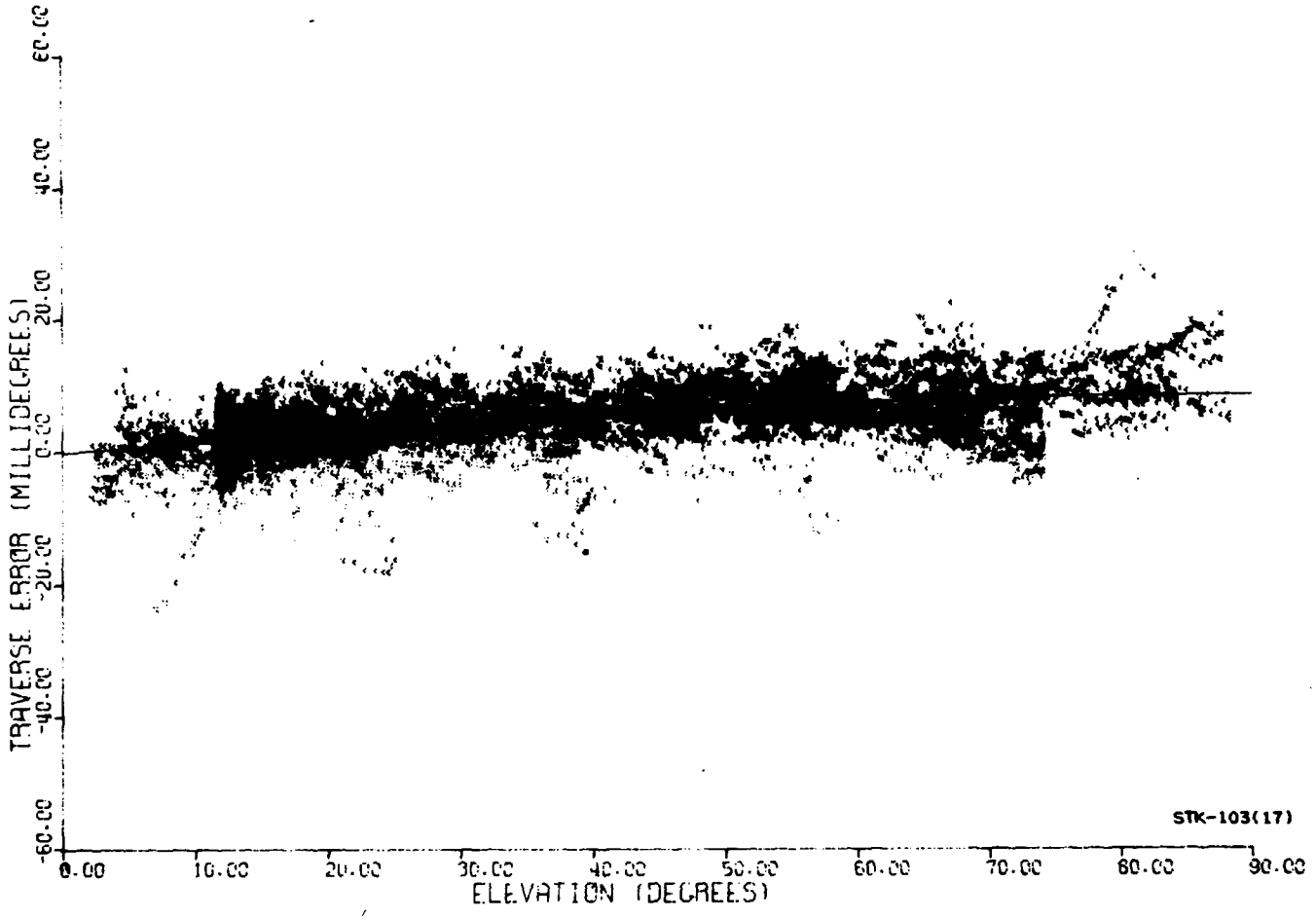

Fig. 17. Comprehensive analysis traverse error model compared with the data after supression of the collimation error, monthly offsets K_A, and rail model.

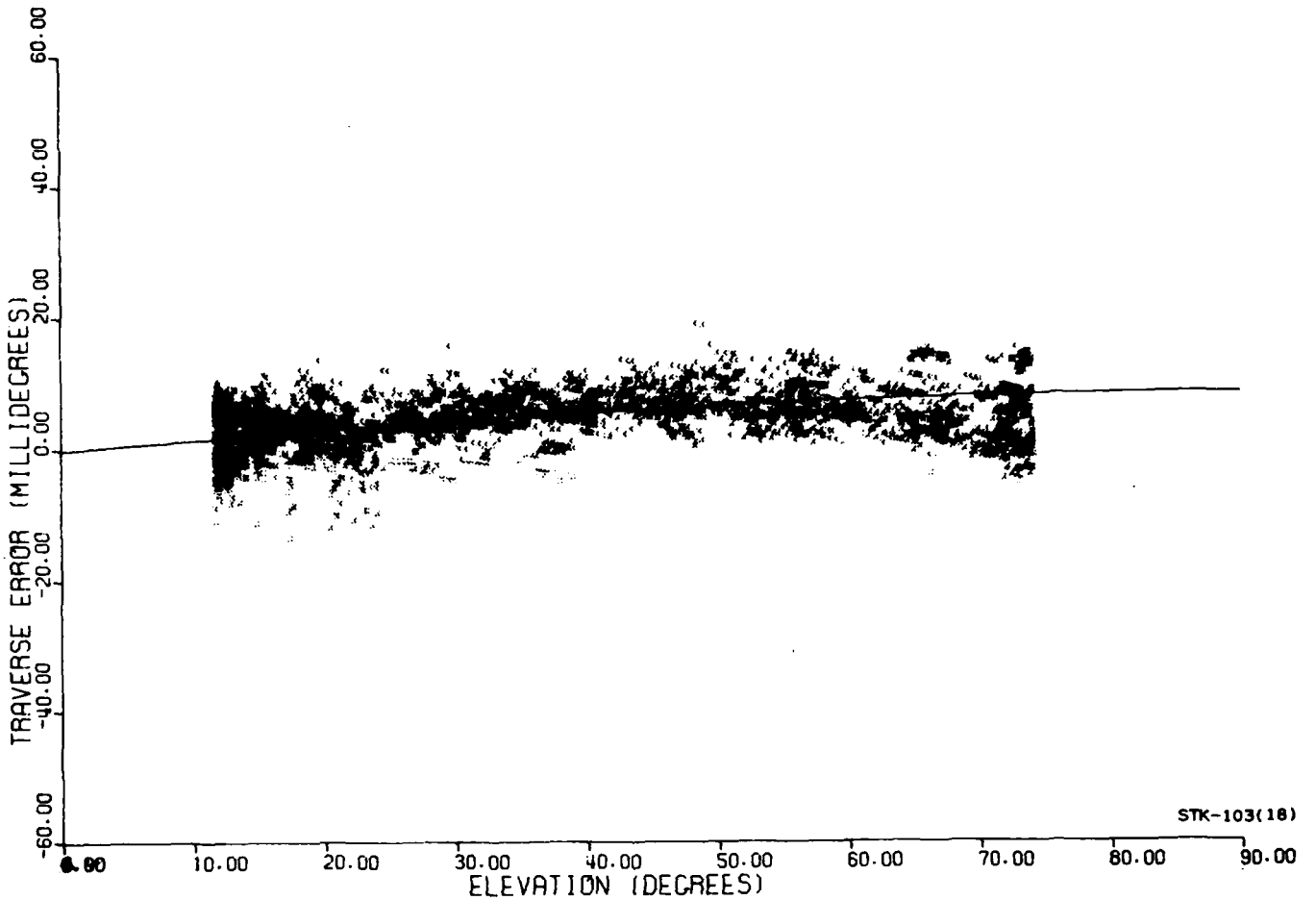

Fig. 18. Same as Figure 17, showing only Cassiopeia data.

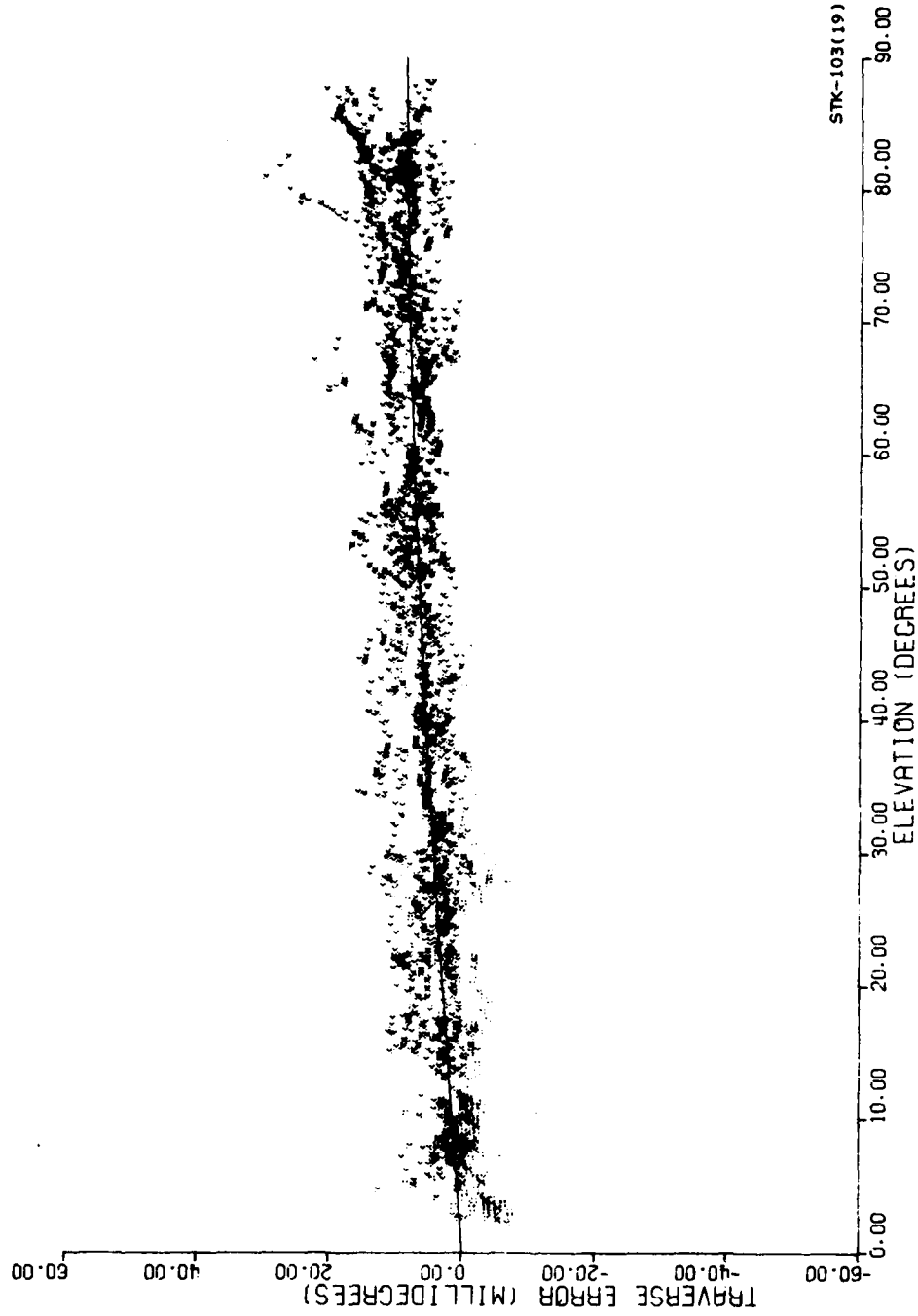

Fig. 19. Same as Figure 17, showing only Cygnus data.

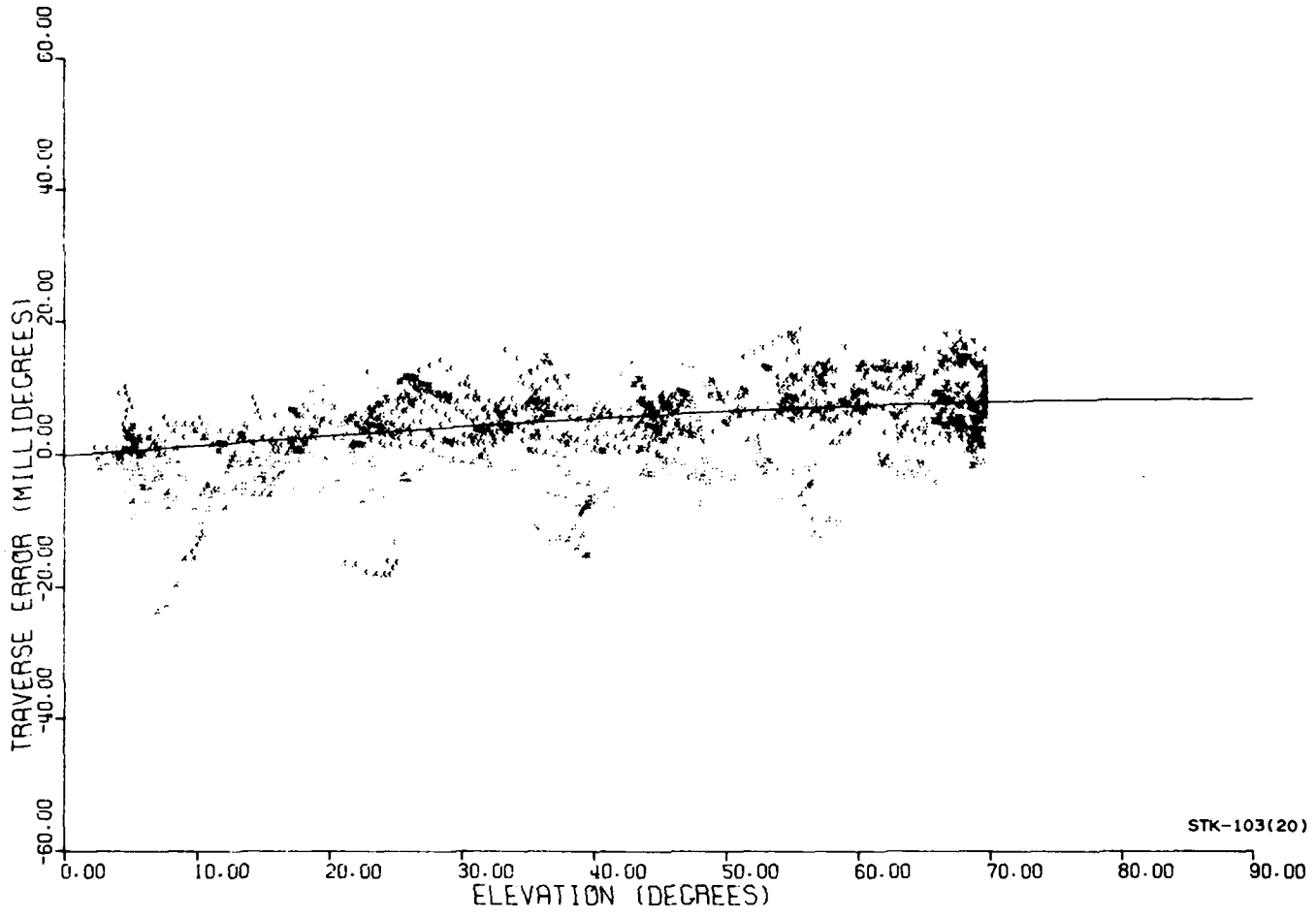

Fig. 20. Same as Figure 17, showing only Taurus data.

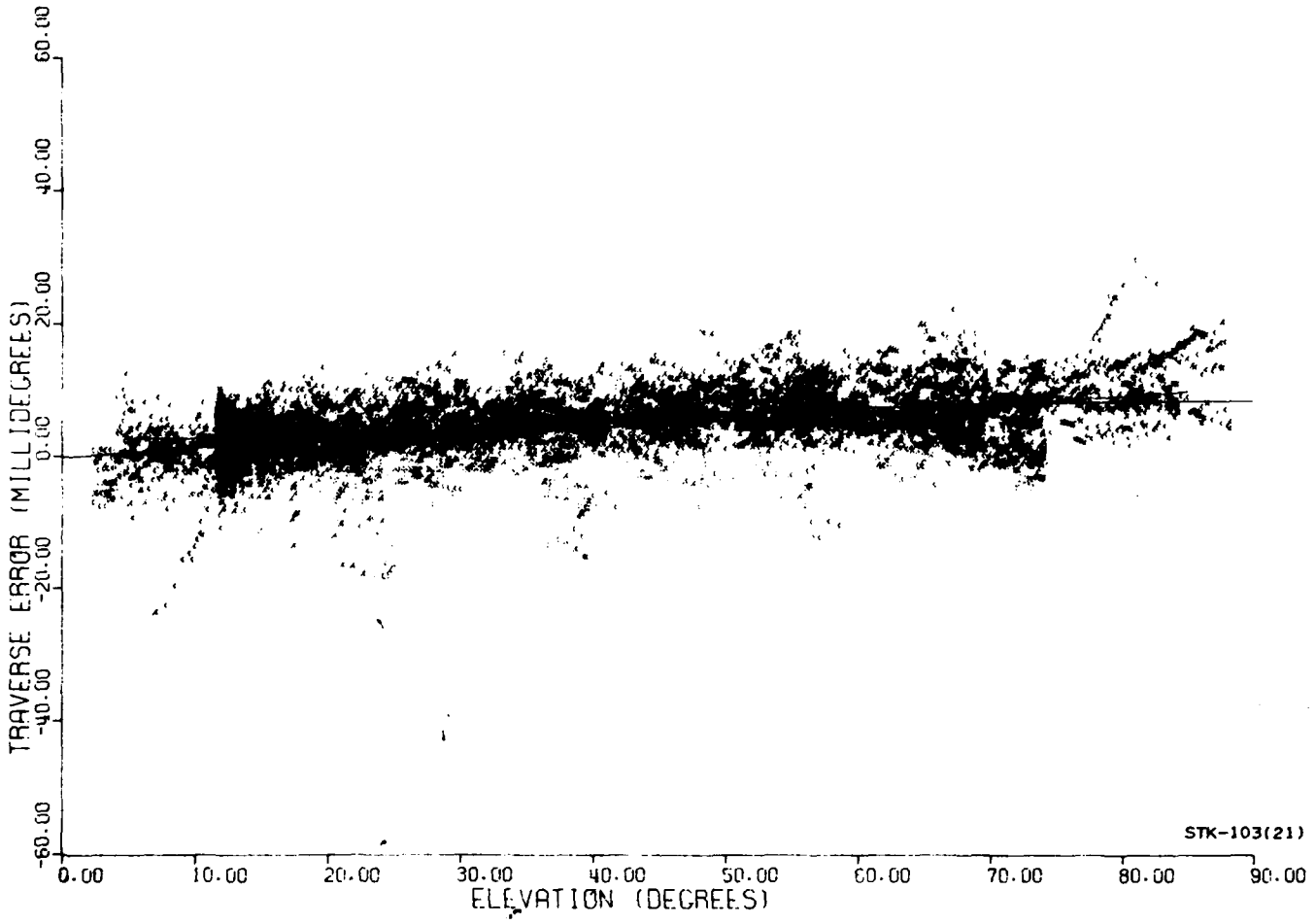

Fig. 21. Model resulting from elimination of ε from traverse error equation.

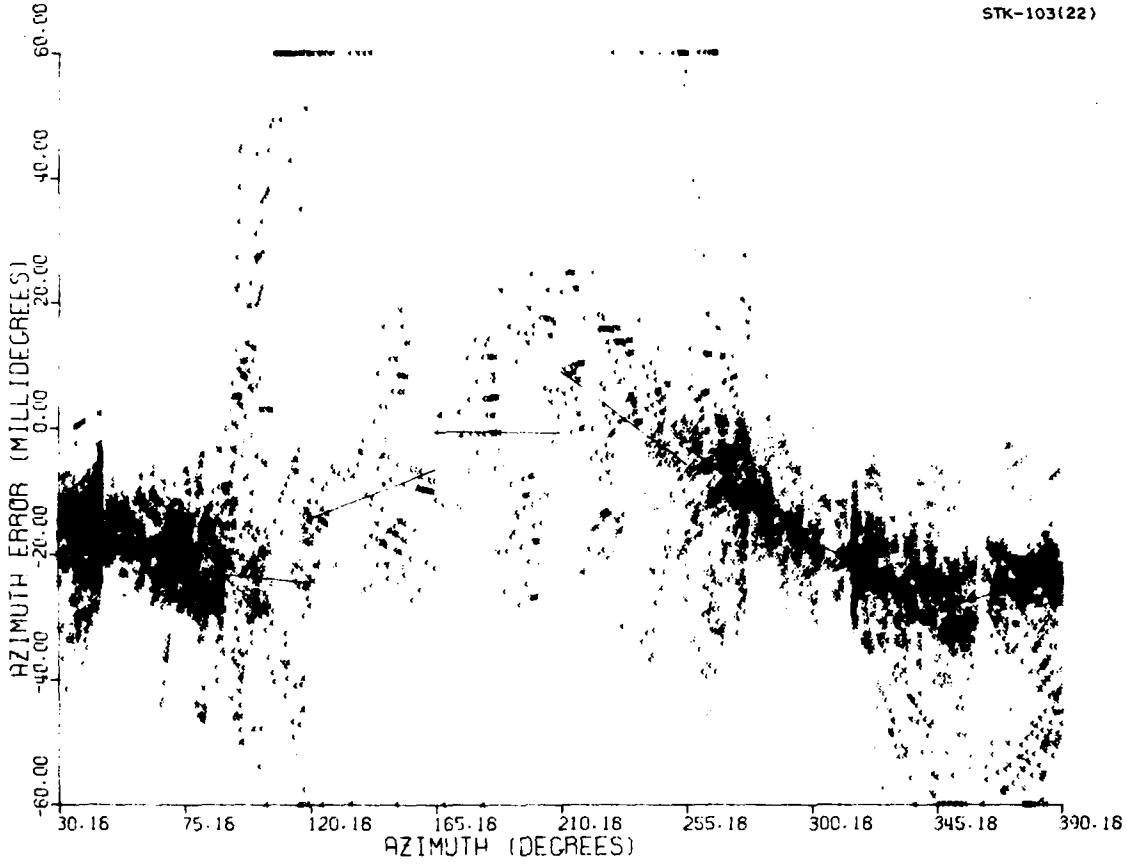

Fig. 22. Comprehensive analysis rail model consisting of eight independent straight line segments (Model 1).

This model will be referred to as Model 1. The standard deviation between the data and the fit for this model is 4.24 mdeg. There is no ideal way to display the data for comparison with this model. Traverse errors are measured whereas the rail model is an azimuth error. What has been done in Figure 22 is first to subtract $\varepsilon \sin E - \delta + K_A \cos E$ from the measured traverse errors and then divide these results by cos E to project them onto the E = 0 plane. This effectively magnifies the data scatter by the factor sec E, and traverse errors acquired at high elevation angles become grossly misrepresented by this projection. It must be remembered, however, that the rail model was not obtained from a fit to the data as shown in this figure but directly from the traverse error measurements. A traverse error obtained at elevation E is in effect weighted as $\cos^2 E$ in determining the rail model (e.g., there is no rail information available from a zenith measurement). If error bars were placed on the "data" points in Figure 22, they would be proportional to sec E (uniform weights were used in the traverse fit). Thus this figure is distorted by the presence of many points of small significance, such as those measurements obtained on Cygnus as it reaches its maximum elevation of 88 degrees at 180° azimuth (see Figure 8). Unfortunately, all of the southern azimuth observations are obtained at relatively high elevation angles on the stars Cygnus and Taurus, and the rail information available on the southern sector rails is thus much inferior to that obtainable to the north.

Figure 23 shows the residual traverse deviations for Model 1 after the entire fitted model has been suppressed. This illustrates that the traverse data are well-fitted and that the large scatter seen in Figure 22 is not an indication of some shortcoming in the model.

A comparison of Model 1 with the three rail models derived from theodolite-telescope measurements (Figure 7) shows some gross features in common but some very different rail detail. The increase at southern azimuths and possibly a secondary increase near north are consistent. But some of the rail slopes are completely in disagreement.

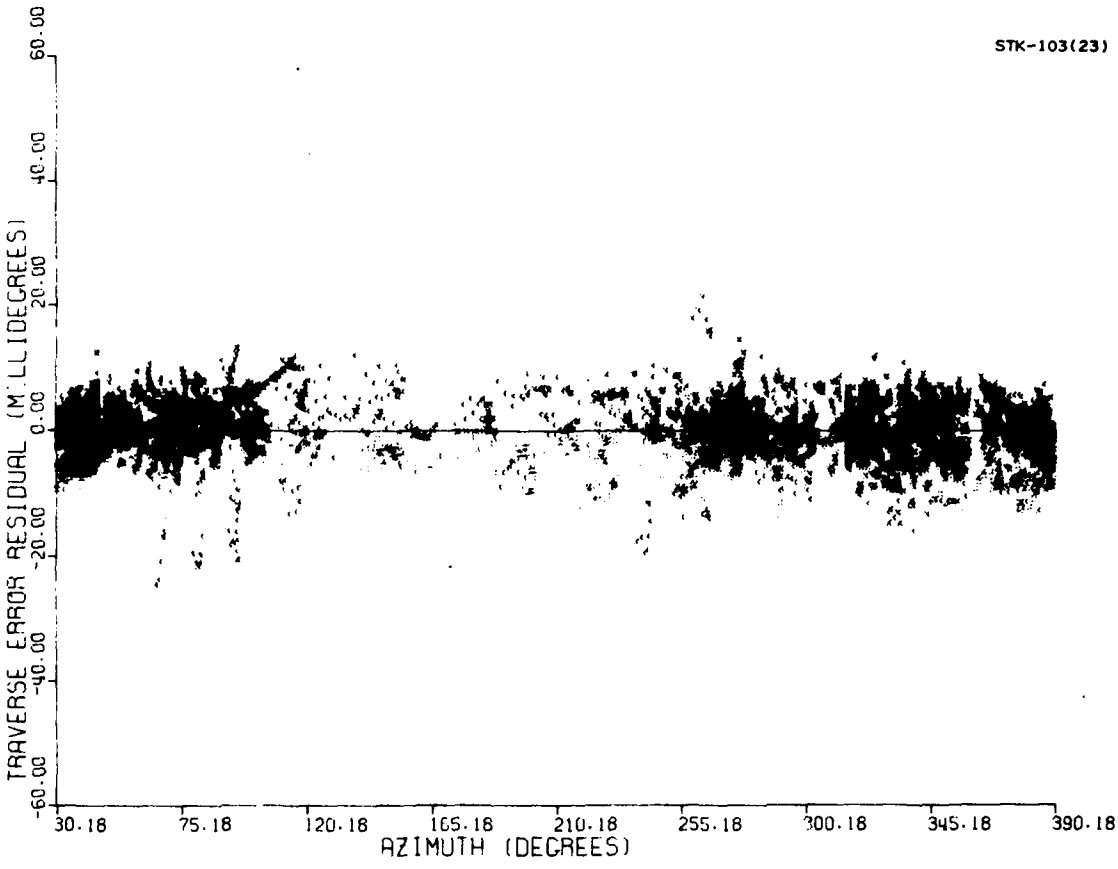

Fig. 23. Traverse error data residuals for Model 1 after subtraction of model variation.

Model 1 appears to show some clearly observable structure in rail offset. The rails certainly are not randomly placed independently of each other. Even their slopes suggest some kind of overriding pattern. The trend seems to be essentially sinusoidal with a smaller second harmonic term. These observations led to further consideration of the rail structure and its offset model.

The cyclic nature of the rail model azimuth variation indicated that there may be some deficiency in its circular geometry. R. H. Wand suggested that perhaps the center of the rail structure was offset from the center of rotation of the antenna azimuth shaft. A. Freed suggested that an overall deformation of the rail geometry, such as a slight ellipticity of the structure, could cause the harmonic term. Appendix A goes through the derivation of the rail model pattern which would result from an offset elliptical rail structure. In the hypothetical case in which the rail structure (and cam-follower) were many sided instead of octagonal, we would have in the limit of a purely elliptical structure a first harmonic sinusoidal rail model component due to a center offset and a second harmonic due to the ellipticity, as originally expected. Insertion of a rail model of the form

$$a \cos A + b \sin A + c \cos 2A + d \sin 2A$$

into Equation 12 in place of the linear rail model, and refitting the entire set of data yielded the rail model shown in Figure 24 (Model 2). It should be realized that all other parameters (ε, δ, K_A) are also somewhat changed by inclusion of new rail model, but these are not major changes. Since the rail model now has zero mean for Model 2, it is possible to derive an independent K_A offset for each FLOPET run, including the first, which was not possible for Model 1, or for any model with unrestricted mean. The harmonic fit to the data appears fairly uniform except, perhaps, at the 30 degree rail corner, where a definite offset appears to occur. The standard deviation between data and fit for Model 2 is 4.55 mdeg.

The next exercise took into account the true octogonal instead of elliptical shape of the rail geometry. If the rails are straight and

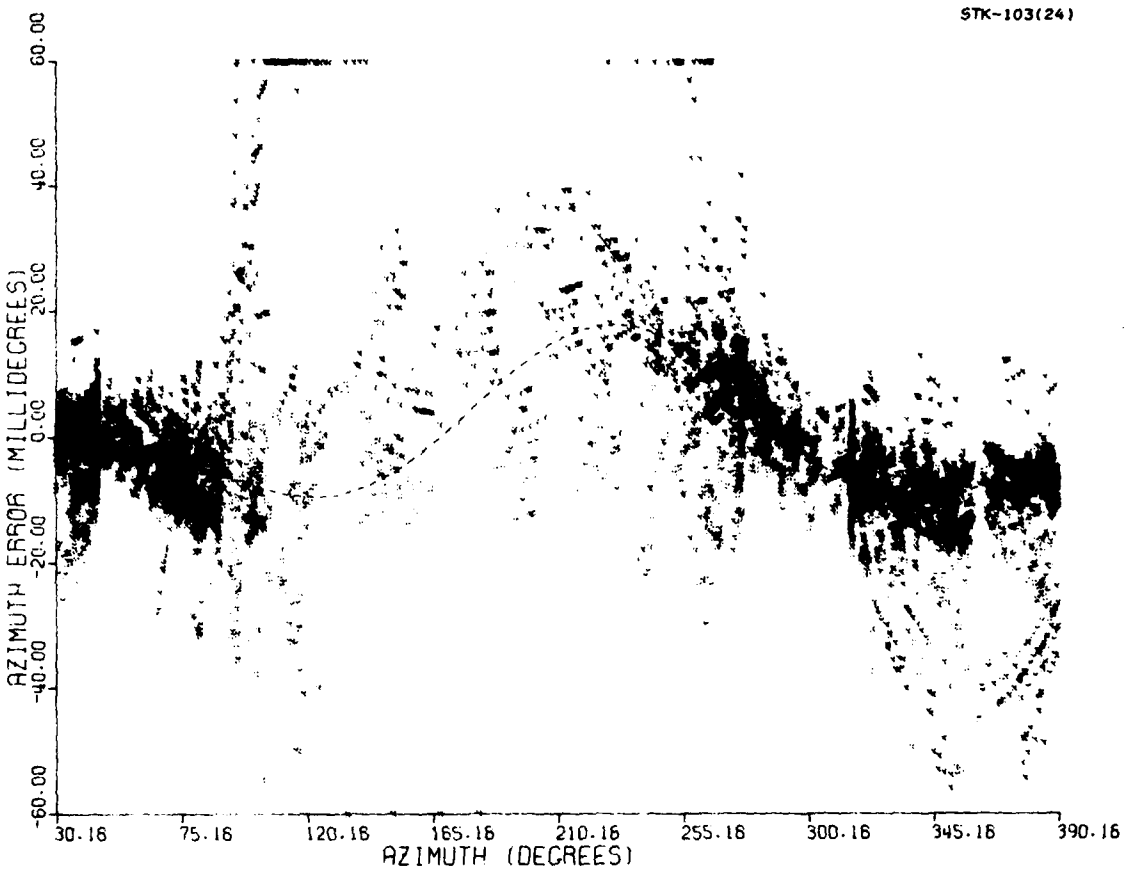

Fig. 24. Comprehensive analysis rail model consisting of a first and a second harmonic sinusoid to simulate the effects of an offset elliptical rail geometry (Model 2).

attached to an elliptical tower perimeter, then the offset incurred on a particular rail will be a constant equal to the value attained by the continuous offset ellipse model somewhere in the rail's azimuth sector. While this offset is generally not precisely equal to the value of the continuous model at the rail midpoint, the 45^{o} sectors and ellipticities are small enough such that only a second-order error is incurred by this assumption. Thus Model 3 is that of a constant offset per rail with the values of the offsets being restrained to lie on a curve composed of the sum of first and second harmonic sinusoids. The result of a fit of this type of rail model to the data is shown in Figure 25. It was found that the fit in this case had a standard deviation of 4.68 mdeg, more than resulted from Model 2 even though a more physically reasonable formulation had been evoked. Apparently, the rails are not quite straight.

Bench tests showed that a worst case error of only 5 mdeg, with a measurement accuracy of 5 mdeg, was incurred due to rail curvature.[2] In their installed position inside the tower perimeter, however, the rail structure may be subject to forces sufficient to cause additional deformation. Thus a Model 4 was developed in which rail bow was also considered. Due to the symmetry of the rails, the tangent to a bowed rail edge at the center of the rail should be parallel to the line connecting the rail ends. Thus rail bow will not affect the offset at rail center but impart a positive deviation on one side of center and a negative deviation on the other. If we make the simplest assumption of a parabolic rail with vertex at rail center, then the rail tangent will vary linearly along the rail. Hence we arrive at a straight-line rail model but with the centers of these lines restricted to lie on the sinusoid harmonic curve once again. Imposition of this rail model in the fit produced the result shown in Figure 26. The standard deviation between the data and fit for this model is 4.38 mdeg. The only difference between rail Models 1 and 4 is that for Model 1 the rail lines are completely independent whereas for Model 4 the line centers are required to lie on this sinusoidal harmonic curve. Model 1 gives a smaller standard

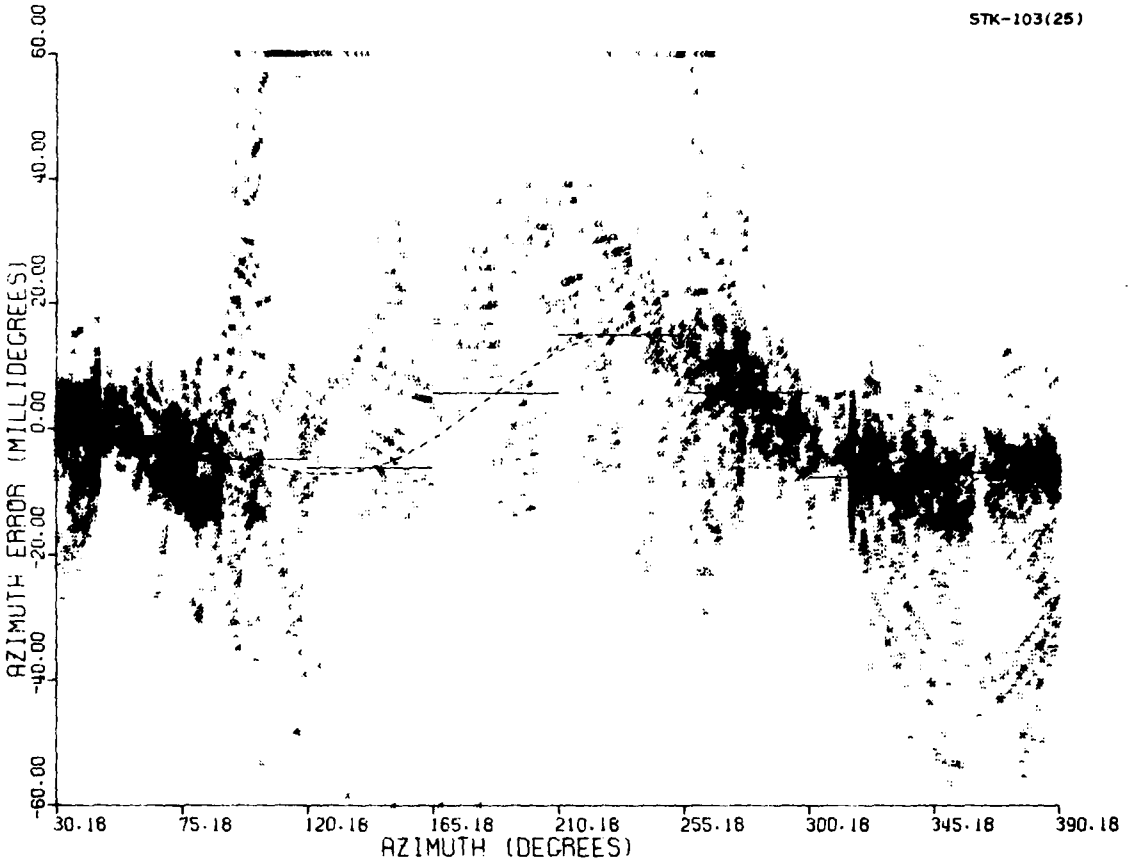

Fig. 25. Comprehensive analysis rail model consisting of a constant offset on each rail with the offsets constrained to lie on a first and second harmonic sinusoid curve at the rail centers (Model 3).

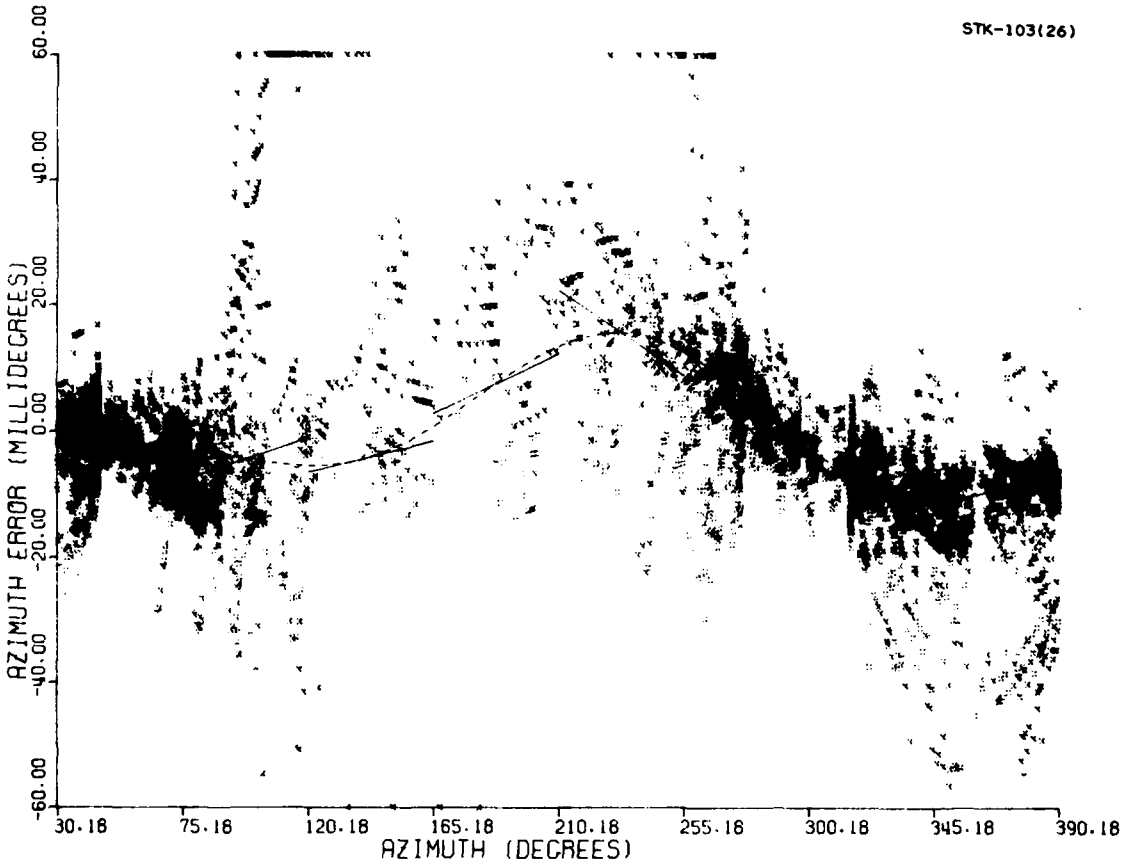

Fig. 26. Comprehensive analysis rail model consisting of eight straight line segments whose centers are constrained to lie on a first and second harmonic sinusoid (Model 4).

deviation, of course, as the rail centers are free to assume optimum positions.

Table 3 summarizes the results of the four types of models fitted to the data. It will be noticed that the rail centers for Models 2, 3, and 4 add to zero while those for Model 1 average -14 mdeg. This is due to the previously explained (arbitrary) assumption for this model that $K_A = 0$ for the first FLOPET run, an assumption necessitated by the non-zero rail model mean allowed by this model (and only this model).

The choice of which of the four rail models presented here to choose for use is rather subjective. Models 2 and 3 require only four parameters for their definition; Model 3 is more closely related to the physical rail geometry, but Model 2 yields a better fit. Models 1 and 4 give better fits than Models 2 and 3 but require 3 and 4 times as many parmeters to describe. The best fit has the least relation to a physical model and the largest number of free parameters. The standard deviation between the data and the fit may be continually decreased, of course, by the addition of more and more terms, but such a brute-force method does not really provide any insight into the underlying structural problem, nor could the degree of complexity of the model be decided upon in any reliable, objective manner. The choice must ultimately be made in considering the effects upon the primary tracking activities of the antenna.

It is interesting to interpret the rail model results in terms of actual mechanical offsets. Model 4 yielded an offset elliptical rail structure pointing bias of (-7.49 cos A -6.06 sin A -2.28 cos 2A + 5.88 sin 2A) mdeg. Appendix A derives the equations for the interpretation of these components in terms of mechanical offsets. The offset between the centers of rotation of the antenna azimuth axis and the rail structure is $(.00749^2 + .00606^2)^{1/2}$ $(\pi/180)$ D = .000168D, where D is the diameter of the rail circle. D is measured to be 1.825 meters such that this offset is 0.31 mm. The direction of this displacement is azimuth $-\tan^{-1}\left[7.49/(-6.06)\right]$, or 231 degrees. The double harmonic term implies that this structure is elongated by the factor $1 + (.00228^2 + .00588^2)^{1/2}$ $(\pi/180)/2 = 1.0000550$ along the azimuth - $1/2 \tan^{-1}$ (2.28/5.88), or 159-339 degrees, and

TABLE 3

COMPREHENSIVE ANALYSIS TRAVERSE MODEL SUMMARY

Rail No.	Model 1 Center	Model 1 Slope	Model 2 Center	Model 3 Center	Model 4 Center	Model 4 Slope
1	-17.51	-.1374	-1.93	-1.33	-3.09	-.1594
2	-23.62	-.0398	-7.22	-4.80	-4.36	.1490
3	-10.31	.1734	-7.37	-6.17	-3.99	.1103
4	- 0.65	-.0070	8.09	5.79	7.59	.2126
5	1.57	-.3275	17.90	15.07	15.63	-.2981
6	-10.37	-.3244	5.92	5.81	5.64	-.3321
7	-22.47	-.1912	-8.60	-7.57	-8.56	-.1465
8	-25.66	.1434	-6.80	-6.80	-8.87	.1357
Parameter						
ε (mdeg)	-24.00		-20.15	-17.04	-21.53	
δ (mdeg)	8.79		12.18	15.09	10.85	
a (mdeg)			-6.50	-5.53	-7.49	
b (mdeg)			-7.51	-6.10	-6.06	
c (mdeg)			-1.49	-2.31	-2.28	
d (mdeg)			7.87	6.49	-5.88	
s.d. (mdeg)	4.24		4.55	4.68	4.38	
number of rail parameters	16		4	4	12	

NOTES:
1. Center is the value of the rail model at rail center (mdeg).
2. Slope is the rail model versus azimuth gradient (mdeg/degrees).
3. a, b, c, d are the values in the azimuth (A) equation a cos A + b sin A + c cos 2A + d sin 2A describing the pointing error due to the offset elliptical distortion of the rail geometry.
4. s.d. is the standard deviation between the data and the fit.

compressed by the same factor along the 69-249 degree azimuth line. This amounts to a 0.05 mm maximum deviation from the nominal circular geometry. The largest rail curvature causes an 7.47 mdeg pointing bias (at the ends of rail 6). It may be easily shown that if the parabolocity of a rail causes a pointing error of $\pm\Delta$ degrees at its endpoints, then the maximum deviation from straightness along the rail is 1/4 tan Δ times the rail length. This amounts to about 0.02 mm for this 7.47 mdeg pointing error for these rails of approximately 0.6985 meters in length.

4.4 Mechanical Modifications: Subreflector Change, Elevation Encoder Realignment, LED Encoder Installation, Tiltmeter Bracket Tightening

The "propagation studies" conducted at Millstone from 1969 to 1973 (see Section 1) used the tracking antenna at both UHF and L-band. Because the UHF capability is not used in the current operations, the frequency-selective subreflector used for these studies was replaced in 1978 (between the May and June FLOPET runs) by the metal Cassegrain subreflector previously used for L-band operation, affording a 1 db sensitivity gain. Such a mechanical modification must necessarily be accompained by a pointing bias change. It is unlikely that the small change in weight would cause important gravitational deflection changes in elevation pointing biases (see Section 2.1.2), but a significant change in collimation error (see Section 2.1.1) would be entirely expected. This will have the effect of a step change in both δ and in the monthly pattern of the K_E variations (Equations 11 and 12). The traverse error (Equation 12) was thus modified to allow for different values of δ to apply before and after the subreflector change. In addition, an electrical realignment of the elevation encoder was made between the January and February 1979 FLOPET runs to try to eliminate the rather large bias (about 0.2 degree) that had existed for many years. Thus the new bias (K_E in Equation 11) was then expected to be near zero.

Inclusion of the post-May 1978 FLOPET runs through the May 1979 run in the analyses described in Section 4.2 yielded a new collimation error δ = -5.60 mdeg instead of the previously found δ = -21.53 mdeg (for Model 4) and K_E and K_A values as shown in Figure 27. The periods of 250, 180, and 0 mdeg K_E offset are evident here. The last eight points on the 250-mdeg plateau form a very stable trend. Between the October and November 1977 FLOPET runs (the first and second of these eight points), a new elevation shaft encoder featuring light-emitting diodes was installed in lieu of the previously used units with incandescent excitation lamps to eliminate the constant adjustments these latter units needed due to continuous decay caused by darkening of the lamps. The 180 and 0 mdeg plateaus are also stable for this same reason, although some still-unexplained anomalous results in the September 1978-February 1979 period (the last 5 points of the 180-mdeg plateau and the first point of the 0-mdeg plateau) caused some increased scatter. The azimuth LED encoder was installed between the November and December 1978 FLOPET runs, and Figure 27 shows K_A to have stabilized thereafter except for the April and May 1979 values which are displaced. This shift was due to a tightening of the single orthogonal tiltmeter bracket screw just prior to the April run. A drift in the output of this tiltmeter had been noticed during preceding antenna tracking usage, and its mounting screw was found to be loose.

4.5 Long-Term and Seasonal Variations, Relative Star Positions

As was mentioned earlier in Section 4.1, the large month-to-month variabilities seen in all model parameters (K_E, β, γ, K_A, ε, δ) as determined from the independent monthly analyses (Figure 10 and 11) led to a suspicion that the "fixed" mechanical pointing offsets might be varying due to continually changing environmental stresses. The comprehensive analysis of Section 4.2, however, showed that three years of data could be fit with better than a 5-mdeg rms residual with constant values of β, γ, ε, and δ applying throughout this period. Examination of the various correlation

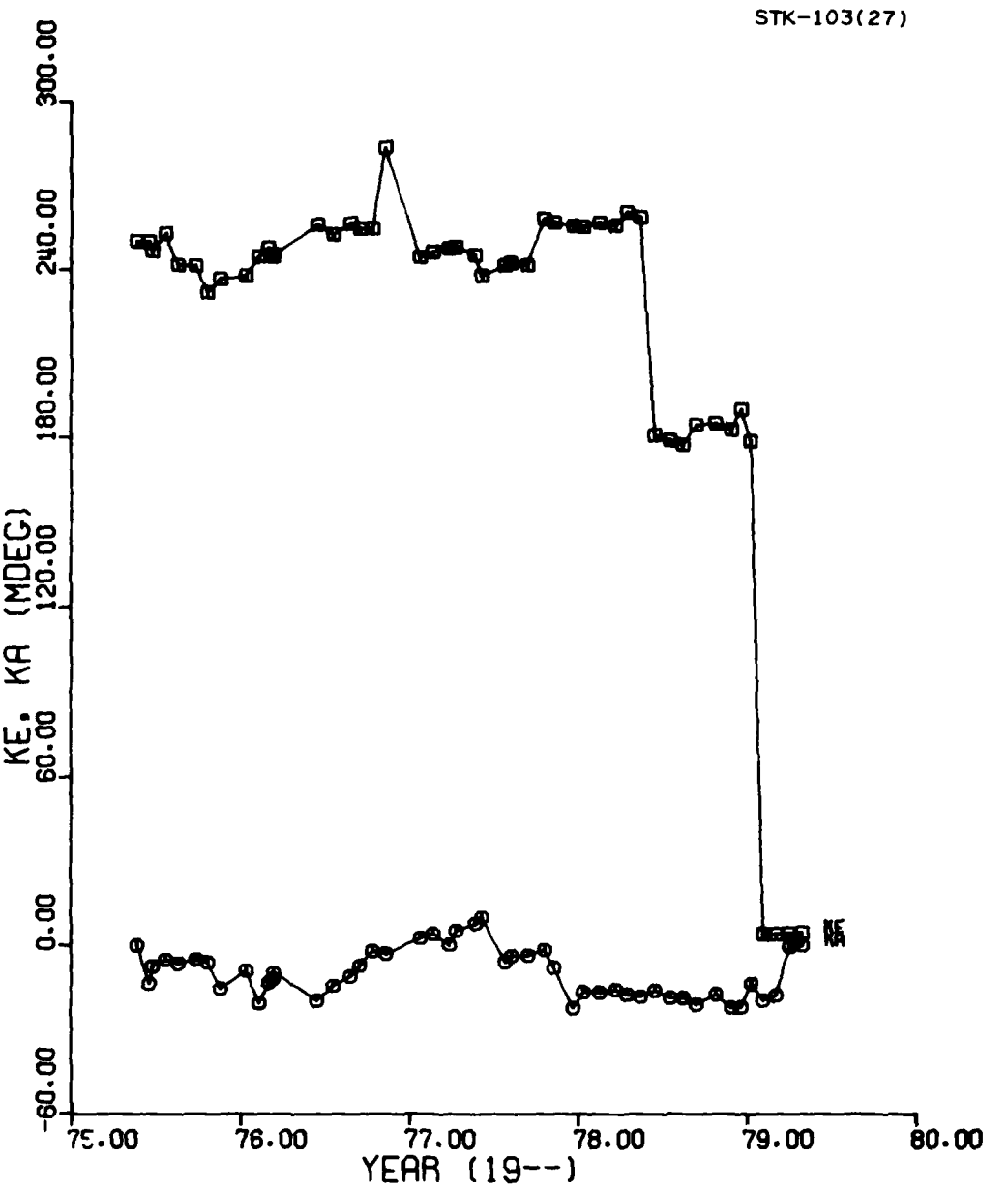

Fig. 27. Comprehensive analysis K_E and K_A results over the period May 1975 - May 1979.

statistics led to the conclusion that there was no evidence that month-to-month changes in these four parameters had occurred, with the exceptions of the known step change in δ caused by the subreflector change (Section 4.4). In addition, comparison of the data month-by-month with the rail model has failed to find any point in time after which a systematic difference between the data and model consistently prevailed on any rail. It appears, then, that the encoder offsets have comprised the only source of long-term fluctuations in the pointing-error model. Since the LED-type encoders have been installed, however, even this source has been largely mitigated (Figure 27).

At the outset of the present study it was expected that a search for seasonal variations in the antenna pointing-error model might prove fruitful due to the sizable changes in thermal stresses which the antenna must go through seasonally. Thus three additional exercises were undertaken in which β and γ, then ε and δ, and then the rail model parameters were allowed simple sinusoidal seasonal variations superimposed upon their constant values. It was soon realized that this type of exercise could produce nothing definitive because of the very high correlation coefficients encountered in these fits. K_A, ε, and δ, for example, were found to be highly mutually correlated in the analysis of Section 4.2. The allowance of a seasonal variation in one of these parameters is seen to render large, compensating seasonal variations in the others. But since K_A is allowed independent monthly values in these analyses, it is effectively already free to assume a seasonal variation, and any subsequent attempt to find seasonal variations in ε, δ, or the rail model is immediately doomed.

It has already been mentioned in Section 3.1 that star positions are known to an accuracy of about 5 arc-sec through interferometer techniques.[5] Background contributions in these reports are generally subtracted out to give the position of the center of the main star, and this could possibly lead to a significant offset between the predicted ephemeris position of the star and the measured error null position of the star plus its background, as

determined by the radar measurements. An attempt was made to investigate the possibility of such offsets by allowing the fit to the FLOPET data to include an independent "collimation error" for each star. Unreasonably large star position biases and a greatly changed rail model resulted from this exercise. This was primarily due to the nearly exclusive determination of the southerly rail sector offsets from Taurus data while these in a heavy preponderance of Cassiopeia data to the north such that relative star positions and the rail offsets could not be simultaneously investigated.

5. SUMMARY

The radio-star calibration program entitled FLOPET has been run monthly since May 1975 to determine and monitor the pointing offsets of the tracking antenna due to mechanical misalignments. The elevation offsets ΔE and traverse offsets ΔT so determined from each of these runs have been fitted by model function of the form

$$\Delta E = K_E + \beta E + \gamma E^2 \tag{13}$$

$$\Delta T = K_A \cos E + \varepsilon \sin E - \delta \tag{14}$$

where E is elevation, K_E and K_A are elevation and azimuth encoder offsets, ε is elevation-axis skew, and δ is collimation error. The ΔE equation is a purely empirical form found to describe adequately the effects of gravitational deflection while the ΔT equation takes expected antenna axis-misalignments into account. In analyses of the monthly observations, the parameters K_E, β, γ, K_A, ε, and δ were seen to fluctuate considerably, arousing suspicion that real changes were taking place in the antenna structure.

The present comprehensive analysis has attempted to combine all FLOPET results collected since May 1975 into one data set to determine if their simultaneous consideration could provide further enlightenment on the antenna pointing offsets. Models of the form of Equations 13 and 14 have

been fit to this data set of more than 10,000 values in each elevation and traverse, maintaining fixed values of β, γ, ε, and δ to apply throughout the period but allowing K_E and K_A to vary monthly to account for the known trim adjustments continually made to the encoders. It was found that each of these data sets could be fit to less than a 5 mdeg rms residual in this manner, indicating that β, γ, ε, and δ had not varied substantially during this period. Inspection of the correlation statistics of these analyses showed inter-parameter correlations with magnitudes up to 98%, for the comprehensive as well as the independent monthly analyses alike, indicating that the large month-to-month variations originally observed resulted from simple mathematical ambiguity instead of real antenna structural variations, and also that even for the comprehensive analysis, the results were not reliable as measures of unamibiguous mechanical offsets. In addition, the installation of LED-type encoder units in November 1977 has virtually eliminated month-to-month encoder variations such that the entire antenna pointing error model has remained virtually unchanged since that time, with the exceptions of those changes which resulted from modifications to the antenna hardware (subreflector change, encoder realignment, tiltmeter tightening).

A second major goal of the comprehensive analysis was to determine if the FLOPET data could aid in calibrating the octagonal rail/cam-follower system used by the tracking antenna as an off-axis azimuth encoder system. To this end the model for the traverse error measurements was allowed to assume a dependence upon rail position with offset allowed to vary linearly along each rail but independently from rail to rail. The result was a "rail model" showing the gross features previously determined by theodolite-telescope measurement but with little of the same detail. It was clear from these results that some overriding pattern prevailed in this rail model, and a consideration of a possible offset between the centers of rotation of the antenna azimuth axis and the rail structure plus a possible ellipticity of the tower perimeter to which the rails were mounted led to the development of a continuous rail model consisting of a first harmonic sinusoid to account for the center offset and a second harmonic for the ellipticity. An

additional exercise maintained this basic geometry but also considered a possible bowing of each rail in a parabolic manner. All of these rail models enabled the FLOPET data to be fit with an rms residual of between 4 and 5 mdeg. In terms of the physical dimensions of these offsets, the model implied a 0.31 mm offset between the azimuth axis and rail octagon center and an out-of-round of 0.05 mm due to tower ellipticity while the most warped rail was bowed 0.02 mm. These mechanical offsets cause maximum pointing offsets of 10, 6, and 7 mdeg, respectively.

APPENDIX A

OFFSET ELLIPSE GEOMETRY

Consider an x,y rectangular coordinate system containing an ellipse centered at (Δx, Δy) with its axes parallel to the coordinate system axes (Figure A-1). This ellipse is described by the locus of (x,y) pairs satisfying the equation

$$\left(\frac{x - \Delta x}{a}\right)^2 + \left(\frac{y - \Delta y}{b}\right)^2 = 1 \qquad \text{(A-1)}$$

where a and b are the half lengths of the ellipse axes in the x and y directions, respectively. For any arbitrary point (x_p, y_p) on this ellipse it is desired to find the angle between two lines passing through (x_p, y_p), one line perpendicular to the ellipse and the other perpendicular to a circle centered at (0,0) This second line must pass through (0,0) . Defining the counterclockwise angles that these lines make with the x axis as α and θ, respectively, we have for θ

$$\tan\theta = \frac{y_p}{x_p} = \frac{\Delta y \pm b\sqrt{1 - (x_p - \Delta x)^2/a^2}}{x_p} \qquad \text{(A-2)}$$

and, considering x as a function of y in Equation A-1, we have for α

$$\tan\alpha = -\left.\frac{d_x}{d_y}\right|_{(x_p,y_p)} = \pm\frac{\sqrt{1 - (x_p - \Delta x)^2/a^2}}{b(x_p - \Delta x)/a^2} \qquad \text{(A-3)}$$

Proper manipulation allows the tan α expression to be reformatted in terms of tan θ

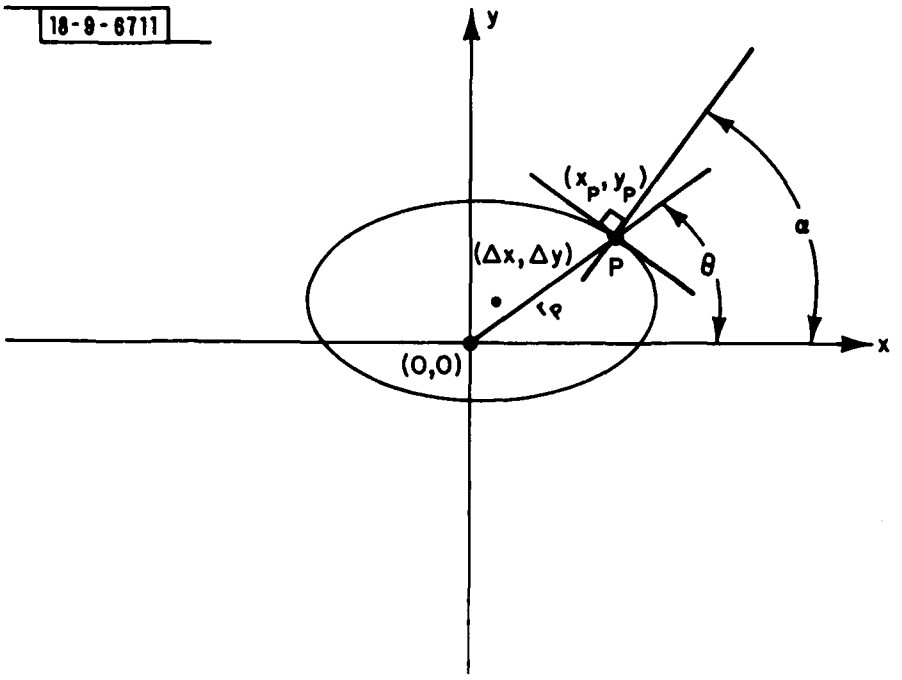

Fig. A1. Offset ellipse geometry.

$$\tan \alpha = \frac{a^2}{b^2}\left(\tan \theta - \frac{\Delta y}{x_p}\right)\left(\frac{1}{1 - \Delta x/x_p}\right) \qquad \text{(A-4)}$$

If α and θ are nearly equal, it becomes useful to write the right hand side of Equation A-4 as tan θ times a quantity near unity

$$\tan \alpha = \tan \theta \left[\frac{a^2}{b^2}\left(1 - \frac{\Delta y}{x_p} \cot \theta\right)\left(\frac{1}{1 - \Delta x/x_p}\right)\right] \qquad \text{(A-5)}$$

Making use of the relation in Figure A-1 that $x_p = r_p \cos \theta$, we have

$$\tan \alpha = \tan \theta \left(\frac{a^2}{b^2} \frac{1 - \Delta y/r_p \sin \theta}{1 - \Delta x/r_p \cos \theta}\right) \qquad \text{(A-6)}$$

This expression can be simplified no further without some assumptions. If we assume our ellipse is only a slight perturbation of a centered circle having radius r, i.e., $r_p \approx r$, then $\Delta x \ll r$, $\Delta y \ll r$, $a = (1 + \varepsilon)r$, $b = (1 - \varepsilon)r$ for some small ε, and Equation A-6 simplifies to

$$\begin{aligned} \tan \alpha &\approx \tan \theta \left[(1 + 4\varepsilon)\left(1 - \frac{\Delta y}{r \sin \theta}\right)\left(1 + \frac{\Delta x}{r \cos \theta}\right)\right] \\ &\approx \tan \theta \left[1 + 4\varepsilon - \frac{\Delta y}{r \sin \theta} + \frac{\Delta x}{r \cos \theta}\right] \end{aligned} \qquad \text{(A-7)}$$

Comparing this with the general relation for small $\Delta\beta$

$$\tan (\beta + \Delta\beta) = \tan \beta + \Delta\beta \frac{\partial \tan \beta}{\partial \beta} = \tan \beta + \frac{\Delta\beta}{\cos^2 \beta}$$

$$= \left(1 + \frac{\Delta\beta}{\sin \beta \cos \beta}\right) \tan \beta \qquad \text{(A-8)}$$

we find

$$\Delta\theta = \alpha - \theta = \left(4\varepsilon - \frac{\Delta y}{r \sin\theta} + \frac{\Delta x}{r \cos\theta}\right)\sin\theta \cos\theta$$

$$= -\frac{\Delta y}{r}\cos\theta + \frac{\Delta x}{r}\sin\theta + 2\varepsilon \sin 2\theta \qquad \text{(A-9)}$$

This expression applies for the ellipse axes aligned with the coordinate axes. For the more general case of arbitrary alignment of the major axis along aximuth $\theta_o - (\theta_o + 180^o)$, we may replace θ by $\theta - \theta_o$ in the second harmonic term of the last equation.

$$\Delta\theta = -\frac{\Delta y}{r}\cos\theta + \frac{\Delta x}{r}\sin\theta + 2\varepsilon \sin 2(\theta-\theta_o) \qquad \text{(A-10)}$$

where θ_o is the counterclockwise angle which the major ellipse axis makes with the x axis (ε is positive for the major axis along θ_o).

To write Equation A-10 linearly in terms of ε and θ_o, it is necessary to expand the second harmonic term

$$\Delta\theta = -\frac{\Delta y}{r}\cos\theta + \frac{\Delta x}{r}\sin\theta + A\cos 2\theta + B\sin 2\theta \qquad \text{(A-11)}$$

where it may be verified that

$$A = -2\varepsilon \sin 2\theta_o \qquad \text{(A-12)}$$

$$B = 2\varepsilon \cos 2\theta_o \qquad \text{(A-13)}$$

$$\varepsilon = \frac{1}{2}\sqrt{A^2 + B^2} \qquad \text{(A-14)}$$

$$\theta_o = \frac{1}{2}\tan^{-1}\frac{-A}{B} \qquad \text{(A-15)}$$

The length of the center offset in terms of the rail radius r is

$$R = \sqrt{\left(\frac{\Delta y}{r}\right)^2 + \left(\frac{\Delta x}{r}\right)^2} \qquad \text{(A-16)}$$

and the direction of this offset counterclockwise from the x axis is

$$\theta_R = \tan^{-1} \frac{\Delta y}{\Delta x} \qquad \text{(A-17)}$$

APPENDIX B

PROCEDURE FOR LARGE, SPARSE, OR WEIGHTED LINEAR LEAST SQUARES PROBLEMS USING GIVENS TRANSFORMS

The method of "least-squares" is a universally-used procedure for the fitting of model functions to observations. In practice, various problems of storage capacity, accuracy, usefulness, efficiency, weighting, model updating, and data editing may be encountered for specific applications. This appendix describes a method based upon Givens[7] transforms as modified and presented by Gentleman[8,9] which provides the following advantages:

1. It is as accurate as any other method.
2. It is as efficient as any other method in the dense matrix case and has provided up to 70% time savings in practical sparse-matrix cases.
3. Zeroes in the matrices are readily exploited in obvious ways to reduce arithmetic cost.
4. Observations may be processed one at a time, relieving the need for large data storage in computer core.
5. The model may be updated by the addition of new observations without redoing previous calculations.
6. Data may be edited out of the model simply by updating with negative weights.

The following is a brief synopsis of the method and its advantages as taken from the papers of Gentleman.

If an nxl vector of observations y and an nxp design matrix X are given, then the model linear least squares problem is to compute a pxl vector of regression coefficients β so as to minimize the sum of the squares of the elements of the nxl residual vector r defined by

$$r = y - X\beta \qquad \text{(B-1)}$$

The solution to this problem is well known to satisfy the normal equations

$$X^T X\beta = X^T y. \tag{B-2}$$

Direct numerical calculations of the cross-product matrix $X^T X$, however, consists of a sequence of operations which is particularly susceptible to quantization error. This defect is overcome by decomposing X into an orthogonal matrix Q and an upper triangular matrix R

$$X = QR \tag{B-3}$$

such that the normal equations are transformed to

$$X^T X\beta = R^T Q^T QR\beta = R^T R\beta = R^T Q^T y \tag{B-4}$$

or

$$R\beta = Q^T y \equiv \theta \tag{B-5}$$

This triangular system is solvable for β without forming the cross-product matrix $X^T X$, and with more accurate results.

A particularly useful way to decompose X and y into R and θ is to apply a sequence of Givens transfromations (plane rotations). A Givens transformation rotating two row vectors

$$0 \ldots 0\ r_i\ r_{i+1} \cdots r_k \cdots$$
$$0 \ldots 0\ x_i\ x_{i+1} \cdots x_k \cdots$$

replaces them with two new row vectors

$$0 \ldots\ 0\ r_i'\ r_{i+1}'\ \ldots\ r_k'\ \ldots$$

$$0 \ldots\ 0\ 0\ \ x_{i+1}'\ \ldots\ x_k'$$

where

$$r_k' = cr_k + sx_k$$

$$x_k' = -sr_k + cx_k$$

$$c^2 + s^2 = 1 \qquad \text{(B-6)}$$

The requirement that x_i transforms to zero indicates

$$r_i' = \sqrt{r_1^2 + x_i^2}$$

$$c = r_i / \sqrt{r_i^2 + x_i^2} = r_i / r_i'$$

$$s = x_i / \sqrt{r_i^2 + x_i^2} = x_i / r_i' \qquad \text{(B-7)}$$

Successive applications of this procedure yield an upper triangular matrix R and a transformed data vector θ, illustrated below for the case p = 4.

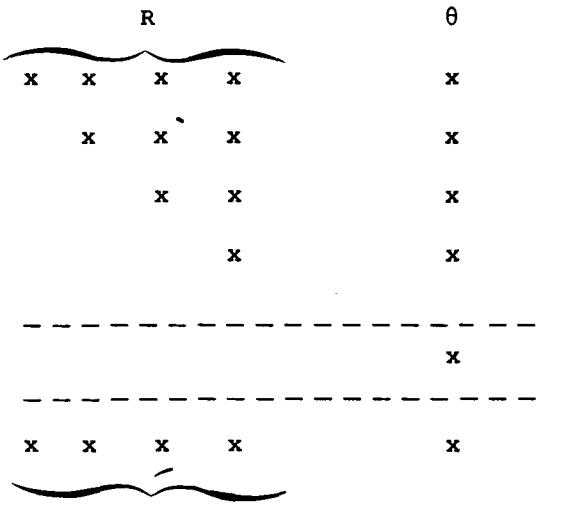

After R has been augmented by a new X row, it can be retriangularized by rotating the new row secessively with the first, second, third, etc., row of R until the entire new row of X has been transformed to zero. If the now-transformed new y element is then rotated with the root residual sum of squares, this residual is updated with whatever is left in the new y element (i.e., residual between data and fit). The new X row and y element are now transformed to zero and may be discarded.

As this process stands, it is rather expensive compared with some other known decomposition techniques (e.g., Householder transformations), but this is just an artifact of the way in which the method is expressed. The trick to avoid square roots altogether and reduce the number of multiplications by one half is to find not R itself but rather a diagonal matrix D and a unit upper triangular matrix $\bar{R}$ such that

$$R = D^{1/2} \bar{R} \qquad \text{(B-8)}$$

Similarly, we have

$$\theta = D^{1/2}\,\bar{\theta} \tag{B-9}$$

and the solution for β is obtained from

$$\bar{R}\beta = \bar{\theta} \tag{B-10}$$

which is at least an easy to solve as Equation B-5. Consider rotating a row of $D^{1/2}\,\bar{R}$ with a scaled row of X (scaling is discussed later).

$$0 \;\ldots\; 0\sqrt{d} \;\ldots\; \sqrt{d}\;\bar{r}_k \;\ldots$$

$$0 \;\ldots\; 0 \;\; \delta x_i \ldots \sqrt{\delta}\, x_k \;\ldots$$

The transformed rows may be written

$$0 \;\ldots\; 0\sqrt{d'} \;\ldots\; \sqrt{d'}\;\bar{r}_k' \;\ldots$$

$$0 \;\ldots\; 0 \;\; 0 \;\ldots\; \sqrt{\delta'}\;x_k' \;\ldots$$

where

$$d' = d + \delta x_i^2$$

$$\delta' = d\delta \,/\, (d + \delta x_i^2) = d\delta \,/\, d'$$

$$\bar{c} = d \,/\, (d + \delta x_i^2) = d \,/\, d'$$

$$\bar{s} = \delta x_i \,/\, (d + \delta x_i^2) = \delta x_i \,/\, d'$$

$$x_k' = x_k - x_i \bar{r}_k$$

$$\bar{r}_k' = \bar{c}\,\bar{r}_k + \bar{s}\,x_k \tag{B-11}$$

That is, the transformed rows can be expressed as a row of a new $D^{1/2}\bar{R}$ and a new scaled row of X, the scaling factor having changed. Storing D and $\bar{R}$ takes no more space than storing R, and the updating formulae (B-11) not only avoid the square roots of (B-6) and (B-7) but upon optimum manipulation, require only half as many multiplications. The retriangularization can thus be done as before, but more cheaply, as cheaply, in fact, as by any other known method.

Although the scaling of the newly included row appears in the formulae to avoid square roots, this actually generalizes the problem to the weighted least squares case, in which not the sum of squares of elements of the residual vector but a weighted sum of squares of these elements is to be minimized, each row having its own weight. The answer to the weighted problem is obtained if each row of X and y is multiplied by the square root of its weight, then the problem solved as in the unweighted case. But this is exactly what happens if the scale factor δ for each row is initialized as the weight instead of unity. In addition, observations are removed simply by reincluding them with their previous weights negated.

Included below are FORTRAN algorithms as developed by Gentlemen[9] to implement these least squares procedures. INCLUD accepts a new observation and updates $\bar{R}$ and $\bar{\theta}$. REGRES may be called at any stage to give the current solution β. Algorithm COV, adapted from Lawson and Hanson,[10] returns the upper-triangular off-diagonal part of the solution covariance matrix in $\bar{R}$ and the variance estimates for β in D. Also included below is a test program to illustrate the use of these algorithms.

```
C
C  ALGORITHM COV, ADAPTED FROM HANSON AND LAWSON, 'SOLVING LEAST SQUARES
C  PROBLEMS,' PRENTICE-HALL, ENGLEWOOD CLIFFS, N. J. (1974).
C
C  GIVEN AN N-TH ORDER UPPER TRIANGULAR MATRIX R WHICH IS STORED SUCH THAT ARRAY
C  D CONTAINS THE DIAGONAL ELEMENTS SQUARED AND ARRAY RBAR CONTAINS THE
C  REMAINING UPPER TRIANGULAR ELEMENTS STORED ROWWISE AFTER DIVISION BY THE ROW
C  DIAGONAL ELEMENT, ALGORITHM COV COMPUTES (R**-1)*(R**-1)**T WITH THE DIAGONAL
C  ELEMENTS STORED ROWWISE IN D AND THE REMAINING UPPER TRIANGULAR ELEMENTS
C  STORED ROWWISE IN RBAR.
C
      SUBROUTINE COV (N, RBAR, D)
      DIMENSION RBAR(1), D(1)
C
C  INVERT THE UPPER TRIANGULAR MATRIX R ONTO ITSELF IN STORAGE.
      DO 10 I=1,N
   10 D(I) = 1./D(I)
      IF (N .EQ. 1) GO TO 90
      NM1=N-1
      DO 30 I=1,NM1
      IJ = (I-1)*(N+N-I)/2 + 1
      RBAR(IJ) = -RBAR(IJ)
      IF (I+2 .GT. N) GO TO 40
      IP2=I+2
      DO 30 J=IP2,N
      IJ = (I-1)*(N+N-I)/2 + J - I
      SM = -RBAR(IJ)
      IP1=I+1
      JM1=J-1
      DO 20 L=IP1,JM1
      IL = (I-1)*(N+N-I)/2 + L - I
      LJ = (L-1)*(N+N-L)/2 + J - L
   20 SM = SM - RBAR(IL)*RBAR(LJ)
   30 RBAR(IJ) = SM
   40 CONTINUE
C
C  FORM THE UPPER TRIANGULAR PART OF THE SYMMETRIC MATRIX (R**-1)(R**-1)**T TO
C  REPLACE R**-1 IN STORAGE.
      NM1=N-1
      DO 80 I=1,NM1
      SM = D(I)
      IP1=I+1
      DO 50 L=IP1,N
      IL = (I-1)*(N+N-I)/2 + L - I
   50 SM = SM + RBAR(IL)*RBAR(IL)*D(L)
      TMP = SM
      IP1=I+1
      DO 70 J=IP1,N
      IJ = (I-1)*(N+N-I)/2 + J - I
      SM = RBAR(IJ)*D(J)
      IF(J+1 .GT. N) GO TO 70
      JP1=J+1
      DO 60 L=JP1,N
      IL = (I-1)*(N+N-I)/2 + L - I
      JL = (J-1)*(N+N-J)/2 + L - J
   60 SM = SM + RBAR(IL)*RBAR(JL)*D(L)
   70 RBAR(IJ) = SM
   80 D(I) = TMP
C
   90 RETURN
      END
```

```
C
C  ALGORITHM REGRES SOLVES THE MATRIX EQUATION RBAR*BETA=THBAR FOR BETA FOR THE
C  SPECIAL CASE IN WHICH RBAR IS A P-TH ORDER UPPER-TRIANGULAR UNIT-DIAGONAL
C  MATRIX STORED ROWWISE.  ONLY THE UPPER-TRIANGULAR OFF-DIAGONAL ELEMENTS ARE
C  ACTUALLY STORED IN THE RBAR ARRAY.  (SEE W. M. GENTLEMAN, J. INST. MATH.
C  APPLICS., 12, 329-336 (1973) AND APPL. STATIST., 23, 448-454 (1974)).
C
      SUBROUTINE REGRES (P, RBAR, THBAR, BETA)
      DIMENSION RBAR(1), THBAR(1), BETA(1)
      INTEGER P
      DO 10 J=1,P
      I = P + 1 - J
      BETA(I) = THBAR(I)
      NR = (I-1)*(P+P-I)/2 + 1
      DO 10 K=I+1,P
      BETA(I) = BETA(I) - RBAR(NR)*BETA(K)
   10 NR = NR + 1
      RETURN
      END
```

```
C
C  GIVEN AN NX1 VECTOR OF OBSERVATIONS Y, AN NX1 VECTOR OF WEIGHTS W, AND AN NXP
C  DESIGN MATRIX X, THE MODEL LINEAR LEAST SQUARES PROBLEM IS TO COMPUTE THE PX1
C  VECTOR OF REGRESSION COEFFICIENTS BETA SO AS TO MINIMIZE THE WEIGHTED SUM OF
C  SQUARES SS OF THE ELEMENTS OF THE NX1 RESIDUAL VECTOR Y-X*BETA.  THIS MAY BE
C  DONE BY FINDING THE DECOMPOSITION X=Q*R, WHERE Q IS ORTHOGONAL AND R UPPER
C  TRIANGULAR, AND SOLVING THE EQUATION R*BETA=Q**T*Y=THETA, OR, MORE
C  EFFICIENTLY, BY SOLVING THE RELATED EQUATION RBAR*BETA=THBAR, WHERE
C  R=D**(1/2)*RBAR, THETA=D**(1/2)*THBAR, D IS DIAGONAL, AND RBAR IS UPPER-
C  TRIANGULAR UNIT-DIAGONAL.  SUCESSIVE CALLS TO ALGORITHM INCLUD WITH A NEW Y
C  ELEMENT , W ELEMENT, AND X ROW CALCULATES D, RBAR, THBAR, AND SS.  D, RBAR,
C  THBAR, AND SS SHOULD BE ZEROED PRIOR TO THE INITIAL CALL TO INCLUD.
C  ALGORITHM REGRES MAY THEN BE CALLED TO FIND BETA AND ALGORITHM COV TO FIND
C  THE BETA COVARIANCE MATRIX.  (SEE W. M. GENTLEMAN, J. INST. MATH. APPLICS.,
C  12, 329-336 (1973) AND APPL. STATIST., 23, 448-454 (1974)).
C
      SUBROUTINE INCLUD(P, WVAL, X, YVAL, D, RBAR, THBAR, SS)
C
C     INCLUDE UPDATES D, RBAR, THBAR AND SS BY THE INCLUSION OF X AND
C     YVAL WITH THE SPECIFIED WEIGHT WVAL.
C
      INTEGER P
      DIMENSION X(1), D(1), RBAR(1), THBAR(1)
      W = WVAL
      Y = YVAL
      DO 20 I=1,P
      IF (W .EQ. 0.0) GO TO 9999
      IF (X(I) .EQ. 0.0) GO TO 20
      XI = X(I)
      DI = D(I)
      DPI = DI + W*XI*XI
      CBAR = DI/DPI
      SBAR = W*XI/DPI
      W = CBAR*W
      D(I) = DPI
      XK = Y
      Y = XK - XI*THBAR(I)
      THBAR(I) = CBAR*THBAR(I) + SBAR*XK
      IF(I .EQ. P) GO TO 20
      NR = (I-1)*(P+P-I)/2 + 1
      DO 10 K=I+1,P
      XK = X(K)
      X(K) = XK - XI*RBAR(NR)
      RBAR(NR) = CBAR*RBAR(NR) + SBAR*XK
   10 NR = NR + 1
   20 CONTINUE
      SS = SS + W*Y*Y
 9999 RETURN
      END
```

```
C
C  TEST PROGRAM FOR ILLUSTRATING THE USAGE OF ALGORITHMS INCLUD, REGRES, AND COV
C  IN A LINEAR LEAST SQUARES PROBLEM.
C
C  FIT A CUBIC TO DEPENDENT VARIABLE Y HAVING WEIGHTS W AS A FUNCTION OF
C  INDEPENDENT VARIABLE Z.
C
      DIMENSION Y(10),W(10),Z(10)
      DIMENSION BETA(4),X(4),D(4),THBAR(4),RBAR(6)
      DATA Y/0., 1., 3., 6., 0., 5., 1., 8., 6., 5./
      DATA W/1., 1., 1., 1., 1., 1., 1., 1., 1., 1./
      DATA Z/0., 1., 2., 3., 4., 5., 6., 7., 8., 9./
      NY=10
      NP=4
      DO 1 I=1,NP
      D(I)=0.
    1 THBAR(I)=0.
      NRBAR=NP*(NP-1)/2
      DO 2 I=1,NRBAR
    2 RBAR(I)=0.
      SS=0.
      DO 3 I=1,NY
      X(1)=1.
      X(2)=Z(I)
      X(3)=Z(I)**2
      X(4)=Z(I)**3
    3 CALL INCLUD(NP,W(I),X,Y(I),D,RBAR,THBAR,SS)
      CALL REGRES(NP,RBAR,THBAR,BETA)
      CALL COV(NP,RBAR,D)
      END
```

REFERENCES

1. P. C. Fritsch, "Final Technical Report: Antenna and RF Circuit Design Millstone Hill Radar," Technical Report 193, Lincoln Laboratory, M.I.T., (7 January 1959); DDC 221688.

2. J. C. Ghiloni (Editor), "Millstone Hill Propagation Study: Instrumentation," Technical Report 507, Lincoln Laboratory, M.I.T., (20 September 1973), DDC AD-775140.

3. J. V. Evans (Editor), "Millstone Hill Propagation Study: Calibration," Technical Report 508, Lincoln Laboratory, M.I.T., (5 October 1973), DDC AD-779689/9.

4. M. L. Meeks, J. S. Ball, and A. B. Hull, "The Pointing Calibration of the Haystack Antenna," Antenna Propag. AP-16, 746 (1968).

5. M. Ryle, B. Elsmore, and A. E. Neville, Nature 205, 1259-1262 (1965).

6. J. V. Evans (Editor), "The Millstone Hill Propagation Study," Technical Note 1969-51, Lincoln Laboratory, M.I.T., (26 September 1969), DDC AD-701939.

7. W. Givens, "Numerical Computation of the Characteristic Values of a Real Symmetric Matrix," Oak Ridge National Laboratory Report ORNL-1574, Oak Ridge, Tennessee (1954).

8. W. M. Gentlemen, "Least Squares Computations by Givens Transforms," J. Inst. Math. Applics., 12, 329 (1973).

9. W. M. Gentlemen, "Basic Procedures for Large, Sparse, or Weighted Least Squares," Appl. Statist., 23, 448 (1974).

10. C. L. Lawson and R. J. Hanson, Solving Least Squares Problems, (Prentice-Hall, 1974).

UNCLASSIFIED

SECURITY CLASSIFICATION OF THIS PAGE *(When Data Entered)*

REPORT DOCUMENTATION PAGE	READ INSTRUCTIONS BEFORE COMPLETING FORM
1. REPORT NUMBER: ESD-TR-79-217	2. GOVT ACCESSION NO. / 3. RECIPIENT'S CATALOG NUMBER
4. TITLE *(and Subtitle)*: Millstone Hill Radio Star Calibration Observations	5. TYPE OF REPORT & PERIOD COVERED: Project Report
	6. PERFORMING ORG. REPORT NUMBER: Project Report STK-103
7. AUTHOR(s): William L. Oliver	8. CONTRACT OR GRANT NUMBER(s): F19628-78-C-0002
9. PERFORMING ORGANIZATION NAME AND ADDRESS: Lincoln Laboratory, M.I.T., P.O. Box 73, Lexington, MA 02173	10. PROGRAM ELEMENT, PROJECT, TASK AREA & WORK UNIT NUMBERS: Program Element No. 31015F
11. CONTROLLING OFFICE NAME AND ADDRESS: Air Force Systems Command, USAF, Andrews AFB, Washington, DC 20331	12. REPORT DATE: 9 August 1979 / 13. NUMBER OF PAGES: 86
14. MONITORING AGENCY NAME & ADDRESS *(if different from Controlling Office)*: Electronic Systems Division, Hanscom AFB, Bedford, MA 01731	15. SECURITY CLASS. *(of this report)*: Unclassified / 15a. DECLASSIFICATION DOWNGRADING SCHEDULE

16. DISTRIBUTION STATEMENT *(of this Report)*

Approved for public release; distribution unlimited.

17. DISTRIBUTION STATEMENT *(of the abstract entered in Block 20, if different from Report)*

18. SUPPLEMENTARY NOTES

None

19. KEY WORDS *(Continue on reverse side if necessary and identify by block number)*

Millstone Hill | Antenna Calibration | Radio Star

20. ABSTRACT *(Continue on reverse side if necessary and identify by block number)*

A comprehensive analyses of all radio-star calibration measurements made since May, 1975, with the Millstone Hill Tracking Antenna is described. No evidence is found to indicate that mechanical offsets in the antenna structure have changed during this period. In addition, it is found that the high stability of the LED-type encoders installed in November, 1977, has virtually eliminated this last source long-term variation in pointing offset.

Calibration of the octagonal rail/cam-follower system used by the Tracking Antenna as an off-axis azimuth encoder system is also investigated. Evidence is presented that the primary pointing errors that arise from inaccuracies in this system are due to an offset between the azimuth axis and the geometric center of the rail octagon, an ellipticity of the tower perimeter upon which the rails are mounted, and a slight bowing of the rails.

DD FORM 1 JAN 73 1473 EDITION OF 1 NOV 65 IS OBSOLETE

UNCLASSIFIED

SECURITY CLASSIFICATION OF THIS PAGE *(When Data Entered)*